

RESEARCH

Open Access



Complement C3a promotes the formation of osteoclasts by inhibiting Sirt1 to activate the PI3K/PDK1/SGK3 pathway in patients with multiple myeloma

Fengjuan Jiang^{1,2,3†}, Yunhe Zhang^{1,2,3†}, Fengping Peng^{1,2,3}, Hui Liu^{1,2,3}, Kai Ding^{1,2,3}, Panpan Cao^{1,2,3}, Xiaohan Liu^{1,2,3}, Lijuan Li^{1,2,3}, Zhaoyun Liu^{1,2,3*}  and Rong Fu^{1,2,3*} 

Abstract

Background Myeloma bone disease (MBD) is the most common complication of multiple myeloma (MM). Our previous study showed that the complement C3a activates osteoclasts to participate in the pathogenesis of MBD; however, its mechanism of action is diverse and complex. Studies have shown that the Sirtuin (Sirt) family of proteins (i.e., Sirt1–7) are expressed in human bone and cartilage, and participate in bone metabolic balance.

Methods and results We measured the levels of complement C3a, Sirt1, osteoclast-related genes, and bone disease-related biological indicators using enzyme-linked immunosorbent assay (ELISA), quantitative real-time PCR and western blotting. Sirt1 expression in osteoclasts was observed to be lower in patients with MM compared to healthy donors and negatively correlated with complement C3a levels, osteoclast-related gene expression, and osteolysis-related markers. Co-immunoprecipitation (Co-IP) and immunostaining were used to verify the interaction between C3a and Sirt1 in RAW264.7 cells. Osteoclasts were then induced from bone marrow mononuclear cells (BMMCs) in patients with MM or cultured RAW264.7 cells, using C3a and/or Sirt1 activator (SRT1720)/inhibitors (EX527) in vitro. Sirt1 inhibits osteoclast formation and complement C3a reverses this inhibitory function of Sirt1 to activate osteoclasts. RAW264.7 cells with induced overexpression or knockdown Sirt1 were transfected with plasmid or shRNA, and RNA-seq analysis was performed. Increased Sirt1 expression resulted in the inhibition of the PI3K/PDK1/SGK3 pathway, which could be reactivated by complement C3a. Sirt1 knockdown activated the PI3K/PDK1/SGK3 pathway, which was further enhanced by complement C3a. A mouse model of MBD was successfully constructed. We injected this model with complement C3a or SRT1720, which further verified that complement C3a can significantly increase the degree of MBD bone damage, whereas SRT1720 can reduce the bone damage aggravated by C3a and treat MBD.

Conclusion We demonstrated that complement C3a interacts with Sirt1 in osteoclasts to participate in the pathogenesis of MBD. Complement C3a promotes osteoclast formation by inhibiting Sirt1 to activate the PI3K/PDK1/SGK3 pathway in patients with MM, which is reduced by treatment with a Sirt1 activator. The application of a Sirt1

[†]Fengjuan Jiang and Yunhe Zhang have contributed equally to this manuscript.

*Correspondence:

Zhaoyun Liu
liuzhaoyun114@163.com
Rong Fu
furong8369@tmu.edu.cn

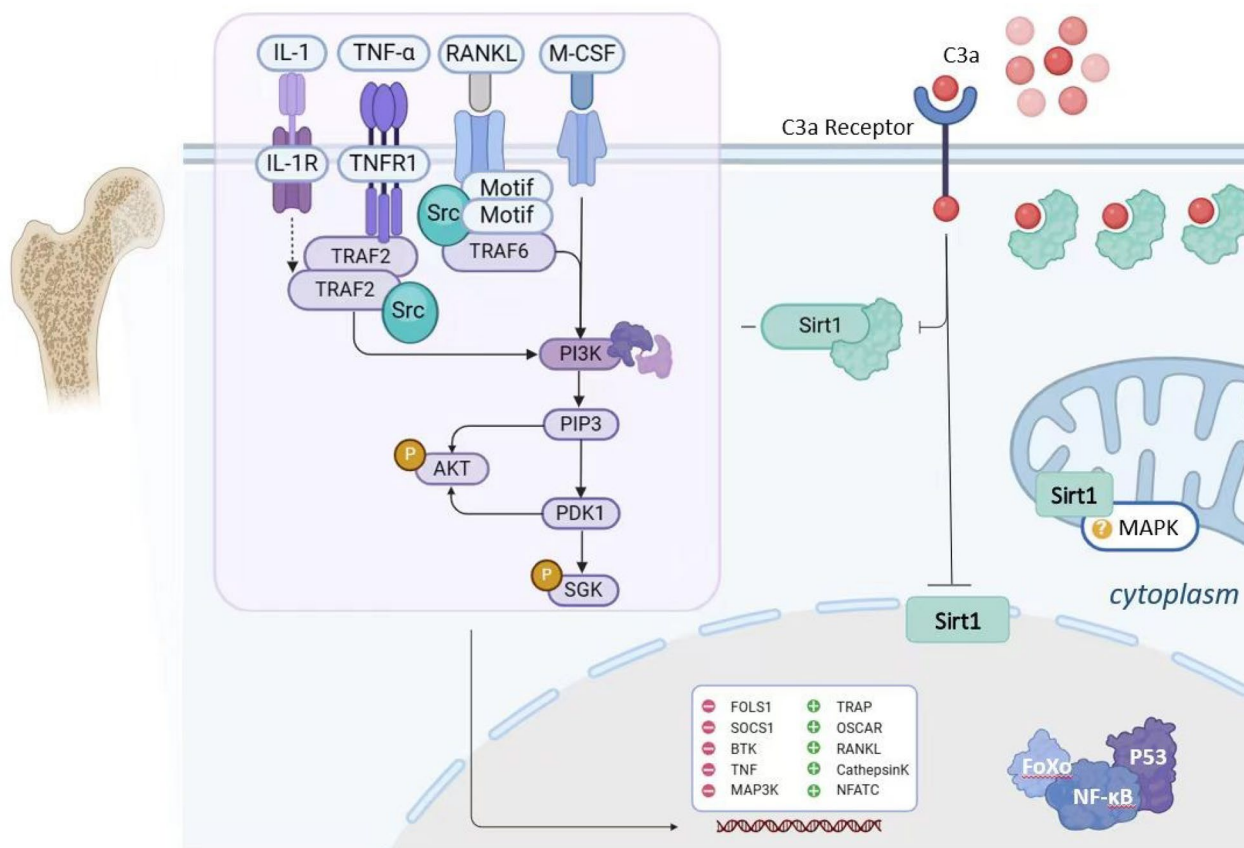
Full list of author information is available at the end of the article



activator can reduce the formation of osteoclasts and reduce the severity of bone diseases in vivo and may be useful for the treatment of MBD. This study identified novel potential therapeutic targets and strategies for patients with MBD.

Keywords Complement C3a, Sirt1, Osteoclasts, Multiple myeloma bone disease, SRT1720, EX527

Graphical Abstract



Introduction

Multiple myeloma (MM) is a hematological malignancy characterized by the proliferation of clonal plasma cells in the bone marrow, and it can cause systemic organ function damage, mainly manifesting as bone destruction, hypercalcemia, anemia, kidney damage, and infection [1]. Approximately 80–90% of MM cases are accompanied by bone disease at the time of diagnosis, which represents its main complication. The main manifestations of myeloma bone disease (MBD) are

hypercalcemia, severe osteoporosis, severe bone pain, osteolytic lesions, pathological fractures, and vertebral compression fractures—all of which negatively affect the quality of life and survival of patients [2]. Therefore, it is important to further study the pathogenesis of MBD, to identify diagnostically sensitive biomarkers and new therapeutic targets to treat it.

The pathogenesis of MBD is mainly caused by abnormal activation of osteoclasts, which leads to enhanced bone resorption. The function of osteoblasts is weakened

or lost, ultimately leading to an imbalance in normal bone metabolism [1, 3, 4]. One of the main mechanisms behind this is MM cells directly, or through inducing other cells in the bone marrow microenvironment (such as stromal cells, bone cells, immune cells, and endothelial cells), cause the secretion of various factors that promote osteoclasts and inhibit osteoblasts. These factors are broad, complex, and have not yet been fully elucidated [5]. Studies have shown that the complement system is closely related to bone metabolism, and its effects on bone metabolism have attracted increasing attention in recent years [6]. We have been committed to the study of the pathogenesis of MBD and observed that complement C3a can activate osteoclasts to participate in the pathogenesis of MBD [7, 8]. However, the mechanism behind this is diverse, complex, and merits further exploration.

In recent years, histone deacetylases have been the focus of much research, and their role in the pathogenesis of MBD has received increasing attention. The acetylation homeostasis of histones is regulated by a variety of histone deacetyltransferases (HDACs) and histone acetylases (HATs). According to their structure, function, and activity, HDAC can be divided into four categories: Class I (HDACs 1–3 and 8), Class II (HDACs 4–7, 9, and 10), Class III (Sirt1–7), and Class IV (HDAC 11). In recent years, studies have confirmed that HDACs play an important role in the differentiation and maturation of osteoblasts and osteoclasts, by affecting gene transcription, replication, and repair [9]. HDAC inhibitors (e.g., trichostatin A and sodium butyrate) inhibit the formation of osteoclasts induced by rat bone marrow cells, reduce cathepsin K expression, and induce apoptosis in mature osteoclasts [10]. Sirtuin (Sirt) family proteins (Sirt1–7) are highly conserved nicotinamide adenine dinucleotide (NAD⁺)-dependent family of Class III HDACs. Sirts are expressed in human bone and cartilage and participate in bone metabolic balance. Studies have confirmed that Sirt1 and Sirt6 promote endochondral osteogenesis and that Sirt activators promote bone formation [11]. Sirt1 can inhibit osteoclast differentiation, and knockdown of Sirt1 expression in the osteoclasts of female mice increased NF- κ B activity, osteoclastogenesis, and bone loss [12, 13]. Venkateshaiah et al. used the knockdown of PBEF1 (a rate-limiting enzyme for NAD⁺ synthesis by nicotinamide) to enhance Sirt1 activity and inhibit osteoclast formation in MM. APO866 (a PBEF1 inhibitor) enhances Sirt1 activity and reduces the occurrence of MBD, thus providing a theoretical basis for MBD treatment [14].

Studies have shown that the complement protein C3 is closely related to Sirt1 and that it plays important roles in inflammatory, immune, and neoplastic diseases. Yamamoto et al. [15] used cardiomyocyte-specific Sirt1

knockout mice (CM-Sirt1^{-/-}) and C3 knockout mice (C3^{-/-}) to confirm that cardiac Sirt1 regulates caloric restriction by inhibiting the expression of C3 after ischemia–reperfusion, thus playing a protective role in the heart. Gillum et al. [16] increased the expression of C3 after knockout Sirt1 in low-fat cells and confirmed that Sirt1 decreased the expression of C3 by inhibiting the NF- κ B pathway. Bolasco et al. [17] conducted a genome-wide analysis of purified DNA fragments using chromatin immunoprecipitation and anti-immunoprecipitation Sirt1 antibodies, confirming that the C3 promoter was closely bound to Sirt1. Recent studies have shown that complement itself affects the macrostructure of bone. Deficiencies of complement proteins C3 and C5 lead to thickening of the epiphyseal growth plate, implying delayed endochondral ossification [18]. However bone matrix resorption requires osteoclasts, whose maturation is regulated by the complement system, particularly C3, C3aR and C5aR [19, 20]. It has also been shown that osteoclasts express C3aR, C5aR1 and C5aR2, and that their ligands C3a and C5a significantly enhance osteoclast formation [21, 22]. Therefore, we hypothesized that complement C3a may activate osteoclasts to participate in the pathogenesis of MBD by regulating the expression of Sirt1 in osteoclasts.

Materials and methods

Reagents and antibodies

The details of the antibodies and other reagents used in our experiments are provided in Supplementary Material 1.

Patients and samples

The study cohort consisted of 165 patients diagnosed with Newly Diagnosed Multiple Myeloma (NDMM). All patients were inpatients at the Hematology Department of Tianjin Medical University General Hospital from January 2021 to November 2023. The diagnosis of NDMM was established based on the updated criteria set forth by the International Myeloma Working Group [23, 24]. The study excluded pregnant candidates. It is important to note that this study was not designed as a clinical trial, hence there was no patient attrition involved.

The clinical characteristics of the patients, including gender, age, R-ISS stage, M-component type, β 2-microglobulin levels, hemoglobin (Hb) levels, calcium (Ca) levels, and serum creatinine levels, are detailed in Table 1. The study protocol was approved by the Ethics Committee of Tianjin Medical University with the approval number IRB2020-KY-109, ensuring ethical standards were upheld throughout the research process. An age-matched group of healthy donors (HD) was also included in the study to serve as a control group.

Table 1 Patients' base-line characteristics

	Newly diagnosed multiple myeloma patients (n = 165) (%)
Gender	
Male	97 (58.8)
Female	68 (41.2)
Age (median)	68
Range	34 ~ 83
R-ISS stage	
I	9 (5.4)
II	112 (67.9)
III	44 (26.7)
M-component type	
IgG	81 (49.1)
IgA	37 (22.4)
IgD	1 (0.6)
Light chain only	44 (26.7)
Nonsecretory	2 (1.2)
β_2 -microglobulin	
< 5.5 mg/L	55 (33.3)
\geq 5.5 mg/L	110 (66.7)
Hb	
< 100 g/L	122 (73.9)
\geq 100 g/L	43 (26.1)
Ca	
> 2.75 mmol/l	42 (25.5)
\leq 2.75 mmol/l	123 (74.5)
Serum creatinine	
< 177 μ mol/L	101 (61.2)
\geq 177 μ mol/L	64 (38.8)

R-ISS Revised International Staging System, Hb Hemoglobin

Bone marrow samples were collected from each patient with NDMM and from healthy donors after obtaining their written informed consent. Bone marrow puncture was performed through the posterior superior iliac spine and 10 ml of bone marrow fluid was retained in a sodium heparin anticoagulant tube for experimental purposes. The consent process ensured that all participants were fully informed about the study objectives, procedures, potential risks, and benefits prior to their participation.

Cell culture

The RAW264.7 cell line was purchased from the Cell Bank of the Chinese Academy of Sciences. They were cultured in high-glucose Dulbecco's Modified Eagle's medium (Gibco, USA) supplemented with 10% of FBS (BI, USA) and were incubated at 37 °C with a humidified atmosphere containing 5% CO₂ (Thermo, USA).

Flow cytometry

CD34⁺OCN⁺ cells are routinely regarded as osteoblast precursors (OBPs), and CD14⁺CD16⁺ cells are routinely used as osteoclast precursors (OCPs). Isolated PBMCs (1 × 10⁶ cells) were stained with 20 μ L anti-human CD34-APC (BD Biosciences), anti-human OCN-PE (R&D System, Abingdon, USA), anti-human CD16-FITC (BD Biosciences), anti-human CD14-PE (BD Biosciences) and their isotype control antibodies, in the dark, at 4 °C for 30 min. The cells were then washed twice with PBS. At least 500,000 counts were obtained and analyzed using CytExpert (Beckman CytoFLEX).

Osteoclast cultures

Isolated bone marrow mononuclear cells (BMMCs) or RAW264.7 cells were incubated in a-MEM medium supplemented with 10% FBS, 100 U/mL penicillin and 100 mg/mL streptomycin in the presence of recombinant RANKL (PBMCs, recombinant human 150 ng/mL, Miltenyi Biotec, USA; RAW264.7 cell line, recombinant mouse 100 ng/mL, Miltenyi Biotec, USA), recombinant macrophage colony-stimulating factor (M-CSF; PBMCs, recombinant human 50 ng/mL, Miltenyi Biotec, USA; RAW264.7 cell line, recombinant mouse 50 ng/mL, Miltenyi Biotec, USA) and recombinant human/mouse complement C3a (Human complement C3a, Emd Millipore, Burlington, MA, USA; Mouse complement C3a, R&D System, USA) at 1 μ g/mL, followed by seeding in a 24-well plate at 1 × 10⁶ cells/well, according to a previously described protocol [7, 8, 25]. The RAW264.7 or patient-derived cells were divided into different wells with varying concentrations of SRT1720 (TargetMol, USA) at 0.5 μ M, 1 μ M, 1.5 μ M, 2 μ M, or 0 μ M DMSO; and EX527 (TargetMol, USA) at 5 μ M, 10 μ M, 15 μ M, 20 μ M, 50 μ M or 0 μ M DMSO; according to previous studies on the effect of SRT1720/EX527 [26, 27].

TRAP staining

Osteoclasts were identified using a TRAP staining kit (Sigma-Aldrich, St. Louis, MO, USA) according to the manufacturer's instructions, as previously described [7, 8]. Briefly, 0.5 mL of Fast Garnet GBC base solution and 0.5 mL of sodium nitrite solution were added to a tube and mixed by gentle inversion for 30 s. Then, 100 μ L of the resulting mixture was mixed with 4.5 mL of deionized water, 50 μ L of naphthol AS-BI phosphate solution, 200 μ L of acetate solution, and 100 μ L of tartrate solution to a final volume of 10 mL in a tube. The 12-well plates with osteoclasts were fixed by immersing in fixative solution for 30 s. Finally, 500 μ L of the mixed solution was added to each well and incubated 10 min in a water bath at 37 °C in the dark. After 10 min, the plates were rinsed thoroughly in deionized water and evaluated

microscopically. Purple multinucleated cells (≥ 3 nuclei) were defined as osteoclasts.

Transfection of shRNA and plasmid DNA

In this project, lipo3000 and LipoRNAiMAX transfection reagents (Invitrogen, US) were used for plasmid transfection and siRNA transfection, respectively, according to the manufacturer's instructions. Transfection was performed using a 6-well plate inoculated with RAW264.7 cells to 70–90% confluency. Next, 10 μg of Sirt1 plasmid or Si-Sirt1 was added to the first EP tube, followed by 250 μL of serum-free and double-antibody DMEM medium. This solution was thoroughly mixed and allowed to stand for 5 min. A 10 μL aliquot of lipo3000 or lipoRNAiMAX was then added to the second EP tube, followed by 250 μL of serum-free and double-antibody DMEM medium, which were again shaken and mixed thoroughly. These two preparations were then mixed, allowed to stand for 30 min at room temperature, and dropped into the well plate. These were incubated at 37 °C in an incubator containing 5% CO₂ for 1–2 h before a few of the transiently transfected cells were collected for the subsequent experiments. The rest of the cells were left for additional culturing under the same conditions. The sequence of Si-Sirt1 used was 5'-AUUAGUGCUACUGGUCUCACUTT-3'.

Quantitative real-time PCR

Quantitative real-time PCR was performed according to a previously described protocol [7, 8]. RNA was extracted from OCs or RAW264.7 cells using TRIzol reagent (Invitrogen, USA), and was reverse-transcribed into cDNA using a cDNA synthesis kit (Vazyme Biotech Co., Ltd., China), following standard protocols. RT-PCR was performed using synthetic primers and SYBR Green (Vazyme Biotech Co., Ltd.). The PCR amplification conditions were as follows: pre-denaturation at 95 °C for 30 s, denaturation at 95 °C for 3 s, and annealing at 60 °C for 10 s, over a total of 40 cycles. The RT-PCR primers used are listed in Supplementary Material 2. The comparative Ct method was used to quantify the relative mRNA concentration. The mRNA values for each gene were normalized to those of internal control (β -actin or GAPDH) and expressed as fold changes relative to the expression of the control. Supplementary material 2: Primer sequences.

RNA-seq analysis

RNA-seq analysis was performed as previously described [8]. First, we conducted RNA-Seq analysis on osteoclasts derived from myeloma patients, with the addition of complement C3a, along with their

corresponding controls. Later we also performed RNA-Seq on RAW264.7 cells overexpressing Sirt1, along with their corresponding control cells. Genes were selected using the criteria for differentially expressed genes (DEGs)—i.e., those with ≥ 1.5 -fold changes of ≥ 1.5 and adjusted P-values of ≤ 0.05 . Relative enrichment and pathway annotation of genes for various functional associations were determined using the Gene Ontology Resource (GO) and Kyoto Encyclopedia of Genes and Genomes (KEGG) pathway databases.

Co-immunoprecipitation

A 1 mL volume of IP dilution buffer was added to the cell sediment, vortexed three times, shaken, mixed, and allowed to rest for 2 min. A 2% cocktail protease inhibitor was then added for 10 min to facilitate complete lysis of the cells. The lysed cells were then centrifuged at 12,000 rpm for 10 min at 4 °C. The supernatant was recovered, leaving 50 μL for input control. The remaining supernatant was divided into 2 tubes—an IP antibody sample tube and an IgG antibody sample tube—which were stored at -80 °C or used for antibody incubation experiments. Next, 100 μL of agarose beads were added to 1 mL of IP buffer, centrifuged at 4,000 rpm for 30 s, washed once, and the supernatant was discarded. IP antibody and IgG (5 μg each) were added to this and incubated at room temperature for 30 min. The supernatant was then transferred to an EP tube containing agarose beads and shaken on a magnetic rack at 4 °C overnight. The following day, the sample was centrifuged at 4,000 rpm for 30 s, after the addition of 1 mL of IP buffer. After washing, 30 μL of loading buffer was added and the sample was cooked at 100 °C for 10 min before being stored at -20 °C for further use in western blot analysis.

Enzyme-linked immunosorbent assay

The bone resorption markers osteocalcin (OCN) and procollagen I amino-terminal propeptide (PINP), bone resorption marker carboxy-terminal cross-linking telopeptide of type I collagen (CTX), and TRACP-5b were measured using ELISA kits (Elabscience, China) according to the manufacturer's instructions.

Western blot

Cultured cells were lysed in RIPA lysis buffer containing protease and phosphatase inhibitor cocktails (Bimake, USA). Lung homogenates and cell lysates were centrifuged at 13,200 rpm for 20 min, and the total protein concentrations of the supernatants were assessed using a BCA assay kit (Beyotime, China). Cytoplasmic and nuclear proteins were extracted using a nuclear extraction kit (Abcam). Equal amounts of the extracted proteins were separated on 8–12% SDS-polyacrylamide

gels and transferred onto PVDF membranes. The membranes were blocked with 5% skim milk and incubated with diluted primary antibodies against Sirt1, PI3K, PDK1, SGK, P-SGK, and GAPDH overnight at 4 °C. The membranes were then washed with 0.1% Tween-20 in Tris-buffered saline (TBS) and incubated with secondary antibodies for 1 h at room temperature, with gentle shaking. Protein bands were visualized using an enhanced chemiluminescence (ECL) kit (Millipore, Billerica, MA, USA), and quantified using ImageJ software.

Mice and treatment

The MBD mouse model was constructed by injecting 15 μL of RPMI-8226 cells (concentration, $5 \times 10^5/\mu\text{L}$) into the bone marrow cavities of the left tibia of NOD/SCID mice, with 15 μL of PBS being injected for the control mice. The mice were sacrificed 7 weeks later for sample collection. Samples of their left tibia were taken, fixed, and imaged via micro-CT. Pathological analysis of the tibia bone marrow was then performed, including H&E, CD138 immunohistochemical, and TRAP staining, to validate the establishment of the MBD model. This was then repeated, and the MBD mice were divided into PBS, C3a injection, Sirt1 activator SRT1720 injection, and C3a/Sirt1 activator SRT1720 injection groups. The following treatments were then performed 4 weeks after the injection of the RPMI-8226 cells.

For the PBS group, an equal volume of PBS was injected intraperitoneally. In the C3a group, tail vein injections of C3a (1.5 μg each, QOD $\times 7$ d) were administered. The SRT1720 group received intraperitoneal injections of SRT1720 (50 mg/kg each, QD $\times 7$ d). The C3a + SRT1720 group was given tail vein injections of C3a (1.5 μg each QOD $\times 7$ d), and intraperitoneal injections of SRT1720 (50 mg/kg, QD $\times 7$ d). The treatments were completed and maintained for 2 weeks. Samples of the left tibia were collected, fixed, and imaged via micro-CT. Pathological analyses of the tibial bone marrow samples were then performed—including H&E staining, CD138 immunohistochemical staining, and TRAP staining—to determine the degree of bone damage.

Statistical analysis

Data analysis was performed using GraphPad Prism 8.0 statistical software. Results are represented as means \pm SDs. Multigroup comparisons were performed using a one-way analysis of variance (ANOVA). Differences between pairs of groups were determined using Dunnett's t-test. Statistical significance was set at $P < 0.05$.

Results

Sirt1 expression in osteoclasts is lower in patients with NDMM than HDs, and negatively correlated with complement C3a levels

All osteoclasts were obtained following the procedure outlined in Fig. 1A. Previous experimental studies have demonstrated that C3a can promote the formation and function of osteoclasts in patients with MM. RNA-seq analysis was performed on the osteoclasts of patients with NDMM treated with 1 $\mu\text{g}/\text{mL}$ C3a or dimethyl sulfoxide, as described previously [7, 8]. Further analysis revealed that the expression levels of histone deacetylase Sirt family proteins (i.e., Sirt1–7) in C3a-activated osteoclasts from patients with MM were significantly lower than those in controls (Fig. 1B). Using PCR for further validation, Sirt1 expression was observed to be significantly reduced in osteoclasts activated by complement C3a (Fig. 1C). Sirt1 expression in osteoclasts derived from patients with NDMM was significantly lower than that in HDs (Fig. 1D). Serum levels of complement C3a in osteoclasts were determined using ELISA. We observed that Sirt1 expression negatively correlated with serum levels of complement C3a in patients with NDMM (Fig. 1E). Therefore, we hypothesized that Sirt1, rather than any other Sirt family members, may be involved in the activation of osteoclasts by complement C3a in patients with MM.

Sirt1 expression in patients with NDMM was negatively correlated with osteoclast-related gene expression and osteolysis-related markers

Previous studies have confirmed that a few biomarkers—such as serum TRACP-5b, OCN, CTX, and PINP levels, and OBP and OCP numbers in the peripheral blood—can effectively reflect the severity of MBD [26, 28]. Therefore, the correlation between Sirt1 expression levels and these MBD-related biomarkers was analyzed. We observed that Sirt1 expression in NDMM was negatively correlated with the number of OCPs and the osteolysis-related marker serum CTX/TRACP-5b (Fig. 1F). However, Sirt1 levels did not correlate with the number of OBPs or the bone formation-related marker serum OCN/PINP. The relative mRNA expression levels of OSCAR/TRAP/RANKL/Cathepsin K genes in patients with NDMM were measured. These were negatively correlated with Sirt1 expression (Fig. 1G). Therefore, we hypothesized that C3a may promote MBD pathogenesis by inhibiting the expression of Sirt1 in osteoclasts, which in turn promotes osteoclast proliferation and function. However, these findings warrant further validation.

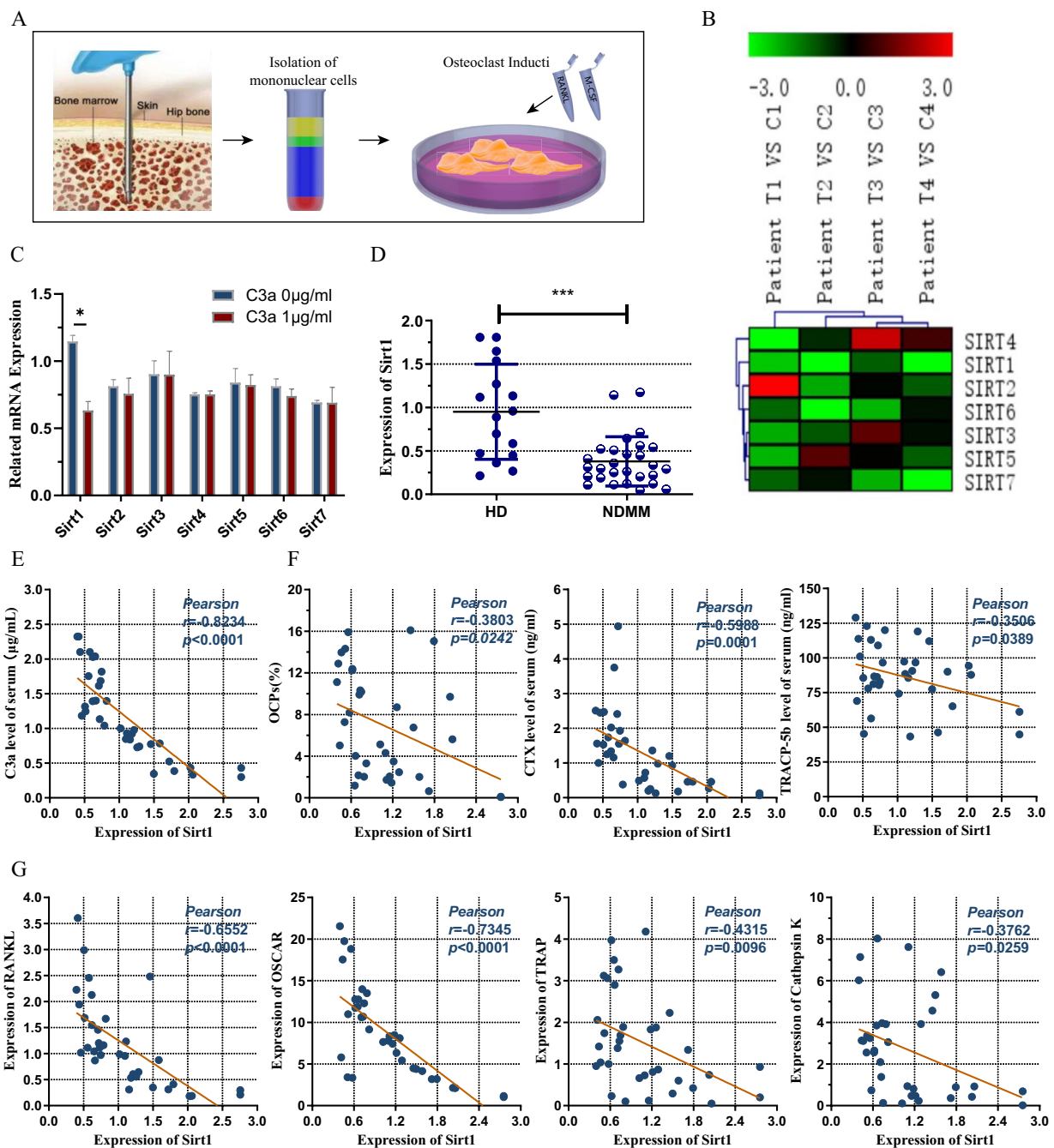


Fig. 1 Sirt1 is involved in osteoclast formation in NDMM and is associated with C3a. **A** Bone marrow single nucleated cells from NDMM were collected by density gradient centrifugation. Recombinant human RANKL (150 ng/ml) recombinant human macrophage colony-stimulating factor M-CSF (50 ng/ml) was subsequently added, and mature adherent osteoclasts were obtained after 14 days. **B** We employed a mainstream hierarchical clustering approach to analyze the FPKM values of genes, applying normalization to the rows (genes) through Z-score standardization. In the heatmap, genes or samples with similar expression patterns are clustered together. The color in each cell represents the normalized value obtained after standardizing the rows of Sirt1-7 expression data, typically ranging from -3 to 3. **C** Sirt1 expression was decreased in the presence of C3a ($P = 0.0134$) but not Sirt2-7. **D** The expression of Sirt1 measured by PCR of OCs in NDMM (0.3789 ± 0.2835) was significantly lower than HD (0.9509 ± 0.5485). ($P < 0.0001$, $t = 4.577$). **E** Sirt1 expression of OCs in NDMM was negatively correlated with serum levels of C3a. **F** Sirt1 expression of OCs in NDMM was negatively correlated with the number of OCPs and the osteolysis-related markers serum CTX/TRACP-5b. **G** Sirt1 expression of OCs in NDMM was negatively correlated with Osteoclast-related genes. The measures taken are from serum samples that are matched with the PCR results of Sirt1 gene expression. Results are shown as mean \pm SD. * $P < 0.05$, ** $P < 0.01$, *** $P < 0.001$

The expression of Sirt1 was decreased in complement C3a-activated osteoclasts, and there was an interaction between complement C3a and Sirt1 in osteoclasts

On the first day of osteoclast culturing, complement C3a was added to the culture system for 14 days of culture maturation. Complement C3a, RANKL, and M-CSF in the culture system were added again every 3 days when the medium was changed. TRAP staining, PCR, and WB were performed after osteoclast maturation. The number and area of osteoclasts in the C3a group were significantly higher than those in the control group (Fig. 2A). C3a promoted osteoclast growth in patients with MM, as has been shown in previous studies as well. The expression of Sirt1 in the C3a-activated osteoclast group was lower than that in the control group, as determined by WB and PCR (Fig. 2B, C). In addition, RAW264.7 cells were used to induce osteoclasts for similar verification. The number and area of osteoclasts in the C3a group were significantly higher than those in the control group (Fig. 2D). The expression of Sirt1 in the C3a-activated osteoclast group was lower than that in the control group, as determined by WB and PCR (Fig. 2E, F). In both the BMMCs from patients with MM and the RAW264.7 cell-induced osteoclasts, we verified that C3a may affect Sirt1. To verify the interaction between C3a and Sirt1, cellular extracts from RAW264.7 cells were collected for co-immunoprecipitation (Co-IP) experiments. Immunoprecipitation (IP) was performed with an antibody against Sirt1, followed by immunoblotting (IB) with an antibody against C3a, showing that C3a was effectively co-immunoprecipitated with Sirt1 (Fig. 2G, left panel). Reciprocally, IP using an antibody against C3a and IB using an antibody against Sirt1 demonstrated that Sirt1 could be pulled down by C3a (Fig. 2G, right panel). Confocal microscopy examination after immunostaining confirmed that C3a was observed mainly in the cytoplasm, and Sirt1 was present in the nucleus and cytoplasm, indicating that C3a and Sirt1 were able to physically interact with one another (Fig. 2H). Therefore, it was concluded that the expression of Sirt1 was decreased in C3a-activated osteoclasts and

that there was an interaction between complement C3a and Sirt1 in osteoclasts derived from patients with MM.

Sirt1 can inhibit the formation of osteoclasts, and complement C3a reverse this inhibitory function of Sirt1 to activate osteoclasts in patients with NDMM

To confirm the effect of Sirt1 on osteoclasts, we added a Sirt1 activator (SRT1720) and a Sirt1 inhibitor (EX527) to the culture to induce osteoclast proliferation from days 1–14 days of culturing. Following the principle of replacing the culture medium every 3 days, the relevant drugs were added whenever the medium was replaced. The optimal concentrations of both drugs were determined by PCR measurement of Sirt1 expression in the resultant osteoclasts. The optimal concentration was determined to be 1 μ M for SRT1720 and 10 μ M for EX527 (Fig. 1H). The number and area of osteoclasts induced in the group treated with the Sirt1 activator (SRT1720) were significantly lower in the cells derived from patients with NDMM compared to the control group (Fig. 3A). In addition, the expression of osteoclast-related genes (i.e., TRAP, RANKL, OSCAR, and Cathepsin K) in the osteoclasts derived from patients with NDMM was significantly lower in the SRT1720 group (Fig. 3E). Similar results were obtained for the osteoclasts induced from the RAW264.7 cells (Fig. 3B, F). Regarding Sirt1 inhibitors, the number and area of osteoclasts induced in the group treated with EX527 were significantly higher than those in the control group derived from patients with NDMM (Fig. 3C). The expression of osteoclast-related genes in the osteoclasts derived from patients with NDMM was significantly increased in the EX527 group (Fig. 3G). Similar results were obtained for the osteoclasts induced from the RAW264.7 cells. (Fig. 3D, H). We observed that Sirt1 activators could suppress the formation of osteoclasts and that the Sirt1 inhibitor promoted it. We observed that Sirt1 inhibited osteoclast formation in the cells derived from patients with NDMM.

Next, we added C3a to the culture system and observed that the number of osteoclasts, fusion area,

(See figure on next page.)

Fig. 2 The expression of Sirt1 was decreased in complement C3a-activated osteoclasts, and there was an interaction between complement C3a and Sirt1 in osteoclasts. **A** Areas of OCs from NDMM (30.15 ± 1.793) were observed by TRAP staining per view. Original magnification: $100\times$ (bar: $100\ \mu\text{m}$). The area of osteoclast fusion was significantly increased by the addition of C3a (18.99 ± 1.220). ($P < 0.0001$, $t = 5.145$) **B** The expressions of Sirt1 in NDMM was detected by Western blot. **C** Relative mRNA expression of Sirt1 in NDMM (3.546 ± 0.7085) was reduced in the presence of C3a (0.9903 ± 0.2172). ($P = 0.0014$, $t = 3.449$) **D** Areas of OCs induced from RAW264.7 cell were observed by TRAP staining per view. Original magnification: $100\times$ (bar: $100\ \mu\text{m}$). The area of osteoclast fusion in RAW264.7 (15.65 ± 0.5771) was significantly increased by the addition of C3a (32.44 ± 5.239). ($P = 0.0333$, $t = 3.186$) **E** The expressions of Sirt1 in osteoclast from RAW264.7 was detected by Western blot. **F** Relative mRNA expression of Sirt1 in osteoclast from RAW264.7 (1.002 ± 0.02959) was reduced in the presence of C3a (0.2793 ± 0.05192). ($P = 0.0003$, $t = 12.10$) **G** Co-immunoprecipitation (Co-IP) assay was performed to demonstrate the interaction between C3a and Sirt1. **H** Immunostaining and confocal microscopy analysis of C3a and Sirt1 subcellular localization (bar: $100\ \mu\text{m}$). **I** The optimal concentrations of SRT1720 and EX527 were selected by PCR in the RAW264.7 cell. Results are shown as mean \pm SEM. * $P < 0.05$, ** $P < 0.01$, *** $P < 0.001$

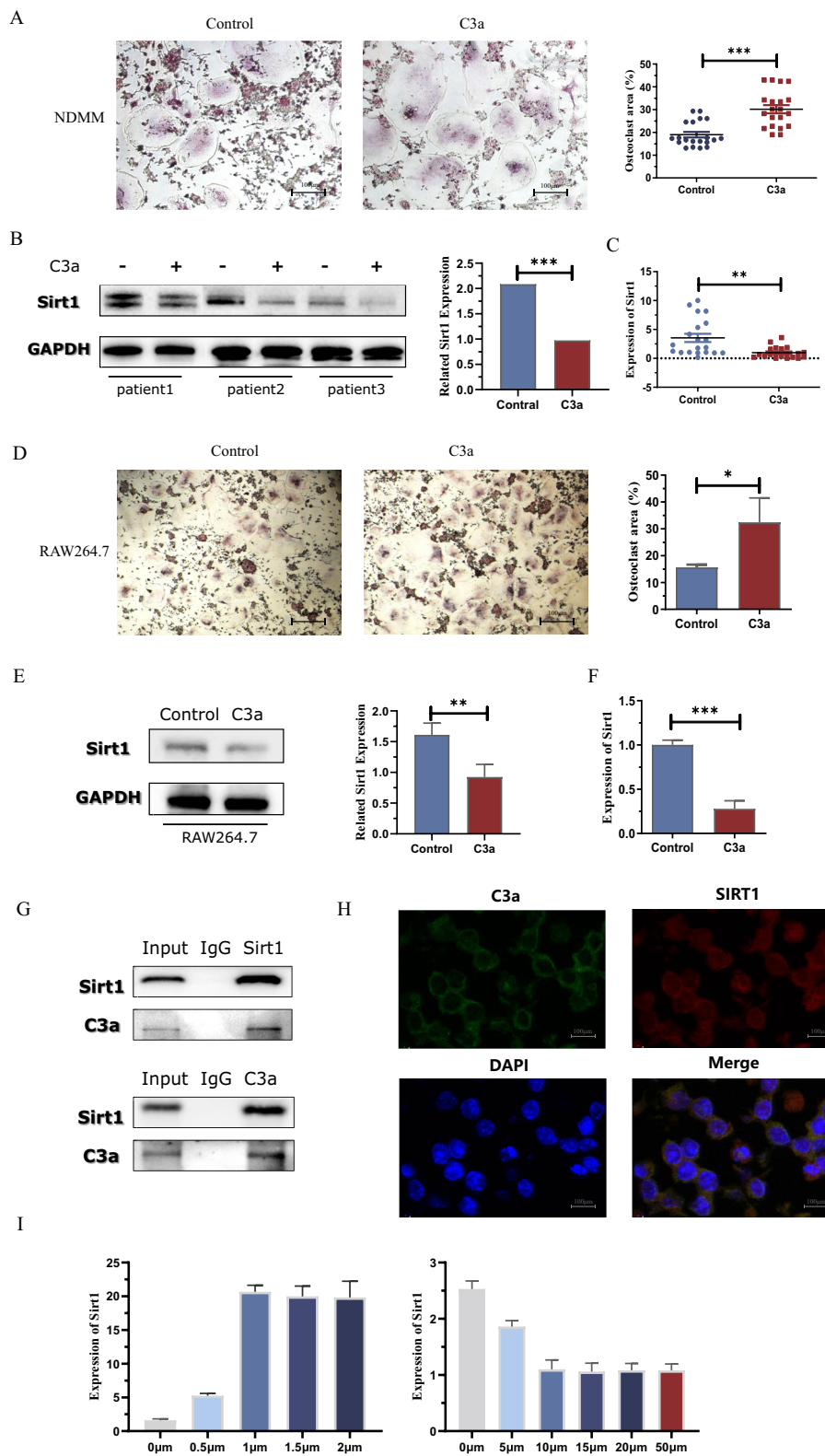


Fig. 2 (See legend on previous page.)

and expression of TRAP/RANKL/OSCAR/Cathepsin K in the osteoclasts derived from patients with NDMM significantly increased in the group treated with both C3a and SRT1720, compared to those treated with SRT1720 alone. However, the promoting effect of C3a only restored the level of osteoclast differentiation to its original state (in the control group) (Fig. 3A, E). Similar results were obtained in the osteoclasts induced from the RAW264.7 cells (Fig. 3B, F). This indicates that C3a can attenuate the inhibitory effect of Sirt1 activators on osteoclasts. By contrast, in the group treated with both C3a and EX527, the number and fusion areas of the osteoclasts were increased (Fig. 3C) and the expression of osteoclast-related genes was elevated, when compared to the EX527 and control groups, in the cells derived from patients with NDMM (Fig. 3G). Similar findings were obtained for the osteoclasts induced from the RAW264.7 cells (Fig. 3D, H). We therefore concluded that C3a and Sirt1 inhibitors act synergistically to promote osteoclast formation. Thus, Sirt1 can inhibit the formation of osteoclasts and complement C3a can reverse this inhibitory effect by activating osteoclasts, in patients with NDMM. Sirt1 is a downstream regulatory protein of C3a that plays a role in osteoclast activation. However, the specific mechanism by which Sirt1 is involved in this regulation remains unclear and merits further study.

Complement C3a promoted the formation of osteoclasts by inhibiting Sirt1 to activate the PI3K/PDK1/SGK3 pathway in patients with NDMM

To further identify the relevant pathways, we performed RNA-seq analysis on the RAW264.7 cells that overexpressed Sirt1 and compared them to the control cells (Fig. 4A, B). The sequencing results have been uploaded to the NCBI database (Accession to cite for these SRT data:PRJNA1123463). We identified a total of 1,367 DEGs between the group that overexpressed Sirt1 and the control groups—including 903 upregulated and 464 downregulated genes (Fig. 4C, D). KEGG pathway analyses were performed by selecting signal transduction-related DEGs from the categorized KEGG pathway maps (Fig. 4E). From the KEGG pathway map, we focused on the top 10 pathways (Fig. 4G). Our previous studies demonstrated that C3a can activate osteoclasts through the PI3K/PDK1/SGK3 pathway; therefore, we focused on the PI3K-AKT and osteoclast differentiation pathways. Further analysis showed that the downregulated genes of the PI3K-AKT pathway after Sirt1 overexpression were PIK3CD, PIK3CA, AKT1, SGK3, LAMB3, PDPK1, COL4A4, COL4A6, LAMB2, TGFA, COL6A2, IRS1, NTRK1, TNC, IL6R, THBS3, GNB3, ITGA7, FGF21, and NGF in the clustering heatmap (Fig. 4H). The downregulated genes in the osteoclast differentiation pathway after Sirt1 overexpression were CREB1, OSCAR, TRAP, ITGB3, CTSK, NFATC1, RANK, NFATC2, and CALCR in the clustering heatmap, indicating that

(See figure on next page.)

Fig. 3 Sirt1 inhibits the formation of osteoclasts, and complement C3a reverse this inhibitory function of Sirt1 to activate osteoclasts in NDMM patients. **A** SRT1720 led to a reduction in osteoclasts from NDMM, but this was reversed to some extent with the addition of C3a. Mean \pm SEM for Control, SRT1720 and SRT1720&C3a are (16.04 \pm 0.7062), (8.381 \pm 0.5928) and (12.64 \pm 1.091) respectively. Control-SRT1720 ($P < 0.0001$, $t = 8.310$) Control-SRT1720&C3a ($P = 0.0127$, $t = 2.615$) SRT1720-SRT1720&C3a ($P = 0.0015$, $t = 3.433$). **C** In the presence of EX527, additional addition of C3a increased the area of osteoclast fusion from NDMM. Mean \pm SEM for Control, EX527 and EX527&C3a are (18.84 \pm 0.1135), (27.13 \pm 0.1.693) and (36.63 \pm 2.179) respectively. Control-EX527 ($P = 0.0006$, $t = 4.118$) Control-EX527&C3a ($P < 0.0001$, $t = 2.238$) EX527-EX527&C3a ($P = 0.0014$, $t = 3.443$). **B, D** The same experiment was performed in osteoclasts from RAW264.7 cell. Mean \pm SEM for Control, SRT1720 and SRT1720&C3a are (16.86 \pm 0.6166), (7.637 \pm 0.8073) and (12.70 \pm 0.5629) respectively. Control-SRT1720 ($P = 0.0019$, $t = 7.290$) Control-SRT1720&C3a ($P = 0.0216$, $t = 3.659$) SRT1720-SRT1720&C3a ($P = 0.0102$, $t = 4.579$). Mean \pm SEM for Control, EX527 and EX527&C3a are (15.65 \pm 0.5771), (30.27 \pm 3.614) and (48.19 \pm 2.692) respectively. Control-EX527 ($P = 0.0187$, $t = 3.823$) Control-EX527&C3a ($P = 0.0003$, $t = 11.82$) EX527-EX527&C3a ($P = 0.0148$, $t = 4.104$). **E, G** The relative expressions of mRNAs of genes TRAP/RANKL/OSCAR/cathepsin K in osteoclasts from NDMM were performed by PCR. SRT1720 (0.8135 \pm 0.1826) (1.050 \pm 0.2876) (1.437 \pm 0.3486) (2.233 \pm 0.5925) -Control (1.861 \pm 0.2466) (2.749 \pm 0.6223) (4.828 \pm 0.8233) (5.747 \pm 1.154) ($P = 0.0016$, $P = 0.0177$, $P = 0.0005$, $P = 0.0101$, respectively) SRT1720&C3a (1.761 \pm 0.2467) (2.767 \pm 0.4317) (4.261 \pm 0.8570) (5.802 \pm 0.9964) -SRT1720 ($P = 0.0038$, $P = 0.0020$, $P = 0.0041$, $P = 0.0038$, respectively) SRT1720&C3a -Control ($P = 0.7743$, $P = 0.9809$, $P = 0.6366$, $P = 0.9713$, respectively). EX527 (1.557 \pm 0.1260) (1.977 \pm 0.1731) (1.656 \pm 0.1077) (1.451 \pm 0.0541) -Control (0.9855 \pm 0.0152) (0.8966 \pm 0.0200) (0.9398 \pm 0.0249) (0.9394 \pm 0.0087) ($P < 0.0001$, $P < 0.0001$, $P < 0.0001$, $P < 0.0001$, respectively) EX527&C3a (2.830 \pm 0.4010) (3.094 \pm 0.4052) (2.109 \pm 0.1475) (1.778 \pm 0.1650) -EX527 ($P = 0.0026$, $P = 0.0124$, $P = 0.0227$, $P = 0.0770$, respectively) EX527&C3a-Control ($P < 0.0001$, $P < 0.0001$, $P < 0.0001$, $P < 0.0001$, respectively). **F, H** The same experiment was performed in osteoclasts from RAW264.7 cell SRT1720 (0.6750 \pm 0.2504) (0.6579 \pm 0.2532) (1.887 \pm 0.1129) (2.173 \pm 0.7950) -Control (2.812 \pm 0.3697) (2.716 \pm 0.3641) (7.629 \pm 1.172) (10.27 \pm 2.651) ($P = 0.0087$, $P = 0.0097$, $P = 0.0082$, $P = 0.0430$, respectively) SRT1720&C3a (2.921 \pm 0.0903) (2.651 \pm 0.4693) (5.480 \pm 0.8143) (9.843 \pm 1.028) -SRT1720 ($P = 0.0011$, $P = 0.0200$, $P = 0.0120$, $P = 0.0041$, respectively) SRT1720&C3a-Control ($P = 0.7880$, $P = 0.9183$, $P = 0.2065$, $P = 0.8882$, respectively). EX527 (1.371 \pm 0.0402) (1.415 \pm 0.2014) (0.5591 \pm 0.1881) (1.070 \pm 0.0298) -Control (0.9202 \pm 0.0927) (1.040 \pm 0.2130) (0.4765 \pm 0.1351) (0.7507 \pm 0.3158) ($P = 0.0111$, $P = 0.2693$, $P = 0.7391$, $P = 0.0018$, respectively) EX527&C3a (1.294 \pm 0.0509) (1.661 \pm 0.0933) (1.764 \pm 0.3600) (1.599 \pm 0.0940) -EX527 ($P = 0.2989$, $P = 0.3310$, $P = 0.0413$, $P = 0.0038$, respectively). Results are shown as mean \pm SEM. * $P < 0.05$, ** $P < 0.01$, *** $P < 0.001$

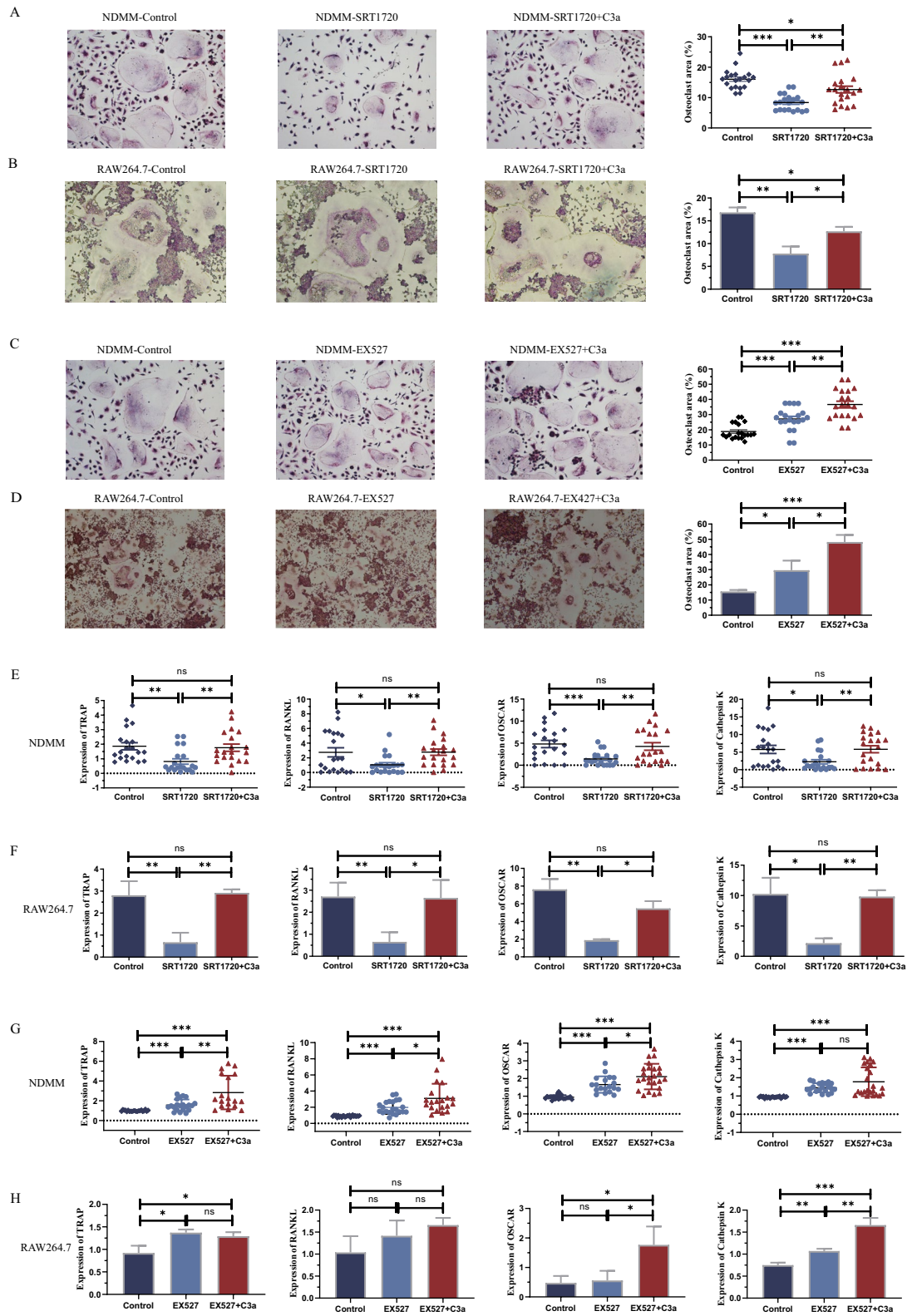


Fig. 3 (See legend on previous page.)

osteoclastosis-related genes were inhibited after Sirt1 overexpression—further verifying the negative effects of Sirt1 on osteoclasts (Fig. 4I). In addition, we performed WB validation for the major proteins in the PI3K-AKT pathway of the RAW264.7 cells to assess overexpression or knockdown of Sirt1 and observed that Sirt1 overexpression resulted in decreased expression of PI3K/PDK1/p-SGK3—which could be reversed by the addition of complement C3a. Sirt1 knockdown increased the expression of PI3K/PDK1/p-SGK3, which was further enhanced by treatment with complement C3a. No changes were observed in AKT or SGK3 levels (Fig. 4J, K).

These results were further verified by the induction of osteoclasts from BMMCs in cells derived from patients with NDMM that were treated with C3a and/or a Sirt1 activator (SRT1720)/inhibitor (EX527). The expression of PI3K, PDK1, SGK3, and p-SGK3 in the EX527 and the complement C3a group were higher than that in the control group. Moreover, the expression of related pathway proteins was higher in the combined group of complement C3a and EX527 (Fig. 5A). The expression of PI3K/PDK1/SGK3/p-SGK3 in the SRT1720 group was significantly lower than that in the control group, and that in the complement C3a group was higher than that in the SRT1720 group (Fig. 5B). However, none of the changes in AKT/p-AKT were significant. Overall, increased Sirt1 expression resulted in the inhibition of the PI3K/PDK1/SGK3 pathway, which could be reactivated by complement C3a. Inhibition of Sirt1 gene expression activated the PI3K/PDK1/SGK3 pathway, which could be enhanced by treatment with complement C3a. We confirmed that complement C3a promoted osteoclast formation by inhibiting Sirt1 to activate the PI3K/PDK1/SGK3 pathway in patients with NDMM.

In the MBD mouse model, complement C3a aggravated the bone disease and Sirt1 activator SRT1720 effectively attenuated it

The MBD mouse model was established by injecting RPMI-8226 cells into the bone marrow cavities of the left tibia of NOD/SCID mice [29, 30]. Myeloma cells in the murine bone marrow were observed using immunohistochemistry (CD138) and H&E staining, at 7 weeks.

CD138+ myeloma cells were stained brown (Fig. 6B), and myeloma cells in the tibia were stained by the H&E staining (Fig. 6C)—confirming that human myeloma cells were injected directly into the bone marrows of the model mice. Moreover, when we observed under 100× microscope, CD138 staining indicated the presence of bone damage in the cortical area near the bone marrow cavity in the MBD group. (Fig. 6B) We observed TRAP staining in the BM and bone disease groups via micro-CT imaging at 7 weeks. TRAP staining, which revealed an increased number of osteoclasts in the tibia, was stronger in the mouse model (Fig. 6D) vs. the controls. We observed the lateral, coronal, and sagittal scans of the mouse tibia (Fig. 6E), and analyzed several 3D parameters to assess bone disease. Bone Mineral Density (BMD) was observed to be decreased in the MBD mouse model, and the bone volume fraction (BV/TV) at 7 weeks was significantly decreased compared to the controls. Decreased trabecular number (Tb.N) and increased trabecular separation (Tb.Sp) were observed (Fig. 6F).

We then divided the MBD mice into MBD (control), C3a injection, Sirt1 activator SRT1720 injection, and C3a/Sirt1 activator SRT1720 injection groups (Fig. 6A). TRAP staining revealed an increased number of osteoclasts in the tibia. In the presence of complement C3a, there were significantly more osteoclasts near the tibial trabeculae, which was alleviated by SRT1720 (Fig. 7A). Micro-CT results for each group are represented in Fig. 7B. Bone destruction was more pronounced in the presence of complement C3a, and the addition of SRT1720 alleviated complement-induced bone disease to a certain extent in the model group (Fig. 7B, C). Comprehensive analysis further verified that complement C3a exacerbated bone disease in mice with MBD, and the Sirt1 activator SRT1720 effectively alleviated bone disease in these mice.

Discussion

Over 80% of patients with MM have varying degrees of bone disease when they are diagnosed, which significantly affects their quality of life and prognoses [31]. Therefore, it is essential to further study the pathogenesis of MBD, identify sensitive biomarkers for its diagnosis,

(See figure on next page.)

Fig. 4 RNA-Seq analysis was performed on the RAW264.7 cells that overexpressed Sirt1 and controls. **A, B** The RAW264.7 cell was transfected using plasmid. The transfection effect was verified by PCR and western blot respectively. (n = 3) **C** There were 903 genes upregulated and 464 genes downregulated in the overexpressed Sirt1 group relative to the control group. **D** Venn diagrams of the three sets of differential gene results. **E** Classification of differential genes under the KEGG pathway. **F** Clustering heat map of differential genes. **G** Differential Gene Enrichment Bubble Maps by KEGG Pathway. **H** Heatmap of PI3K-AKT pathway-related genes. **I** Heat map of osteoclast differentiation genes. **J** Western blot results of RAW264.7 cell overexpressed Sirt1 and knocking down Sirt1 with or without C3a. Validation of PI3K-AKT pathway-related proteins. **K** Results of PCR determination of osteoclast-related genes after overexpression of Sirt1 and knockdown of Sirt1 in RAW264.7 cell. Results are shown as mean ± SD. *P < 0.05, **P < 0.01, ***P < 0.001

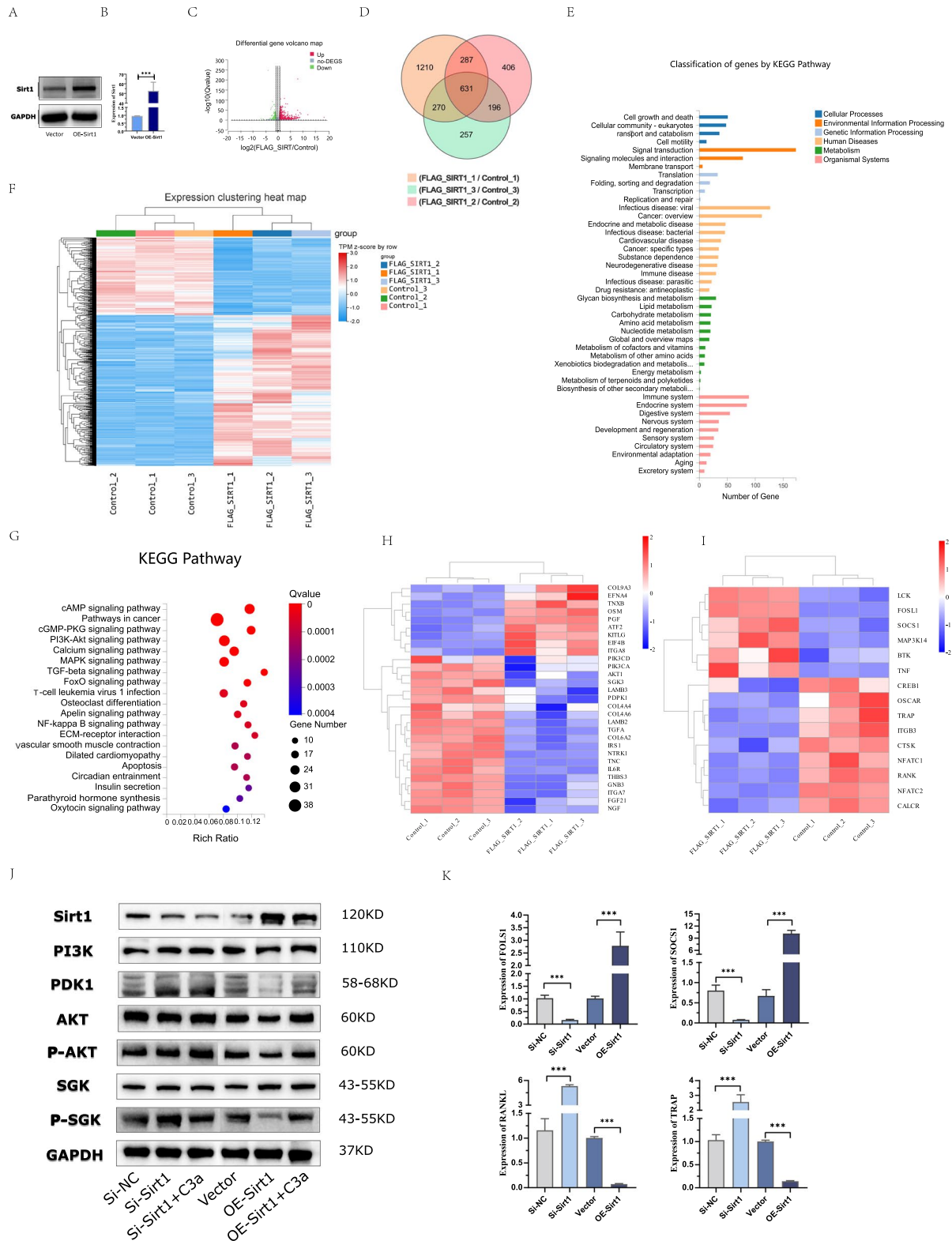


Fig. 4 (See legend on previous page.)

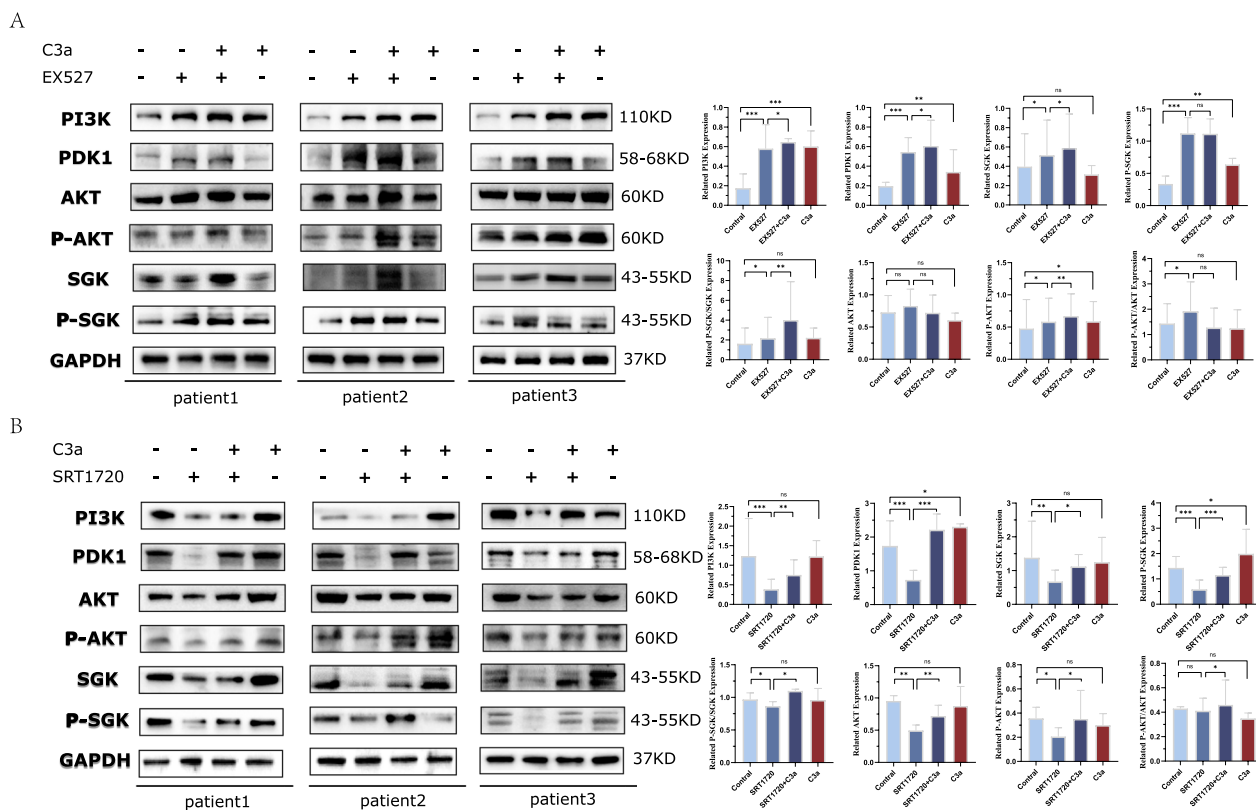


Fig. 5 Complement C3a was verified by western blot to promote osteoclast formation in NDMM patients by inhibiting Sirt1 to activate the PI3K/PDK1/SGK3 pathway. **A** The experimental groupings were EX527-/C3a-, EX527+/C3a-, EX527+/C3a+, EX527-/C3a+ (n=3) **B** The experimental groupings were SRT1720-/C3a-, SRT1720+/C3a-, SRT1720+/C3a+, SRT1720-/C3a+ (n=3). Results are shown as mean ± SD. *P < 0.05, **P < 0.01, ***P < 0.001

and identify new therapeutic targets for its treatment. Previous studies have confirmed that complement C3a activates osteoclasts in patients with MM, leading to the elevated expression of PDK1/SGK3, representing a likely pathogenic mechanism for MBD. To further investigate the mechanisms associated with the C3a-related activation of osteoclasts, we re-analyzed our RNA-seq analysis on the osteoclasts derived from patients with NDMM treated with or without C3a, as described previously. Studies have shown that Sirt-family proteins (Sirt1–7) are expressed in human bone and cartilage, and participate in bone metabolic balance. Therefore, we investigated whether Sirts are involved in MBD. Through our RNA-seq analysis results, we observed that the expression of the Sirt family (Sirt1–7) in C3a-activated osteoclasts derived from patients with MM was significantly lower than that in comparable controls. PCR was performed to further investigate this notion. This revealed that Sirt1 expression was most significantly reduced in osteoclasts activated by complement C3a in patients with NDMM. Of the seven members of the Sirt family, Sirt1 is the well-studied protein in bone and cartilage, and its role in

chondrocytes and osteoclasts is essential for proper skeletal development and homeostasis [11–14]. We therefore targeted Sirt1 and continued to explore its role in osteoclasts.

In other osteoclast specimens derived from patients with NDMM and healthy controls, we measured the expression level of Sirt1. Sirt1 expression was observed to be significantly lower in patients with myeloma than in healthy controls. We measured the expression of bone disease-related biomarkers in patients with NDMM. OCPs are attracted from the bone marrow to the bloodstream by chemokines, or recruited for resorption in the bone [26]. CTX-I is released during mature osteolysis, and TRACP-5b is thought to reflect osteoclast cell activity—both of which are considered important markers for detecting bone resorption and homeostasis [26, 32]. Many studies have confirmed that a few biomarkers—such as serum TRACP-5b [33], OCN [34], CTX [35], and PINP [36] levels, and OCP [26] and OBP [37] numbers in the peripheral blood, may effectively reflect MBD severity. Similar to other osteoblast-related genes, our PCR results suggested that Sirt1 gene expression

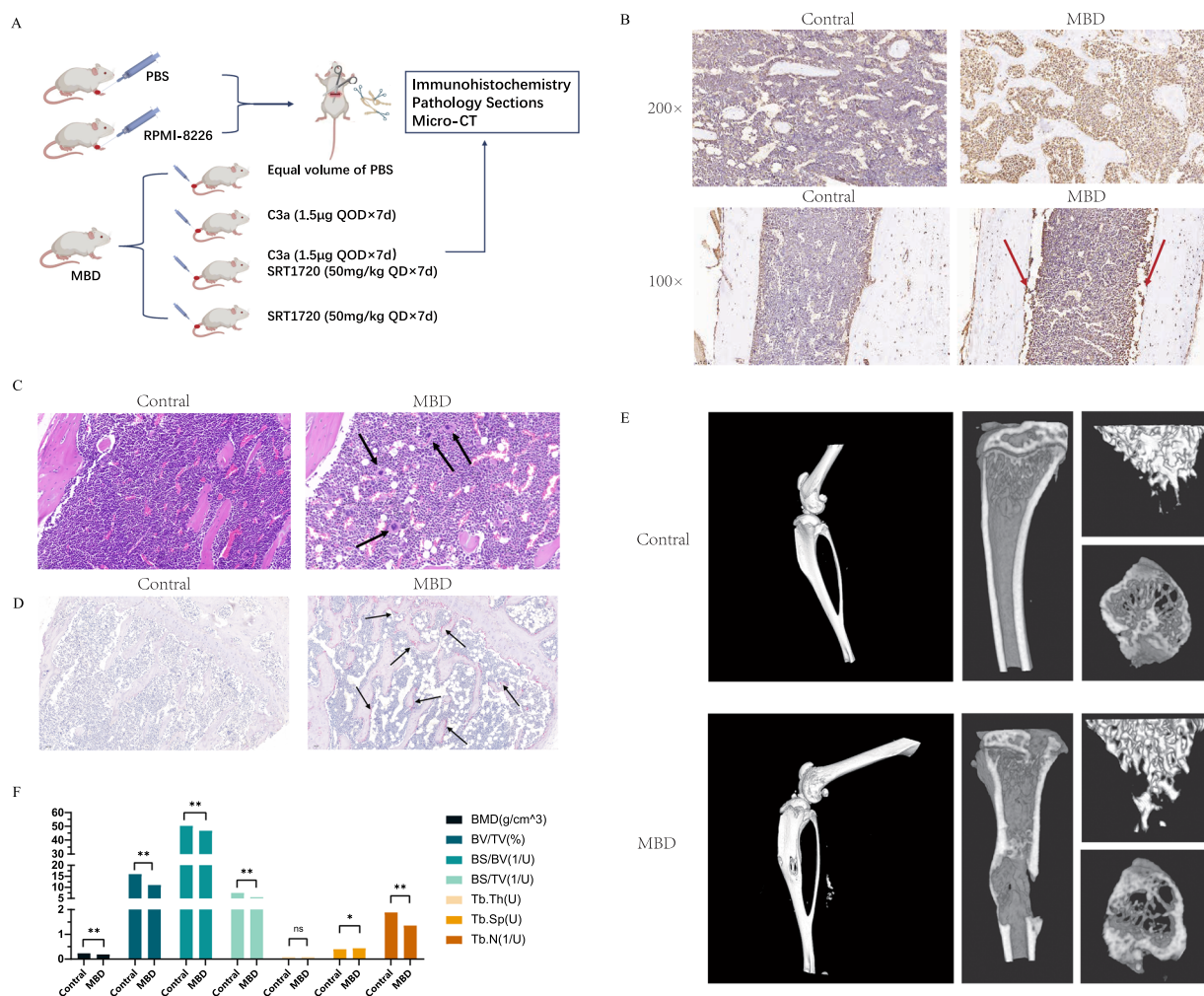


Fig. 6 The MBD mouse model was constructed by injecting RPMI-8226 cells into the bone marrow cavity of the left tibia of NOD/SCID mice. **A** Schematic model for the MBD mouse study. Myeloma cells (RPMI-8226) were injected directly into the marrow space of right tibiae of NOD/SCID mice, PBS injected into mice as controls. Experimental groupings are shown, as well as the dose and duration of administration of C3a and SRT1720. **B** 7 weeks after injection, the mouse model showed positive brown staining for CD138 immunohistochemistry, while the control group was negative. (200 × & 100 ×). **C** Myeloma cells in BM were observed by H&E staining in the mouse model at 7 weeks after injection compared with controls (200 ×). **D** TRAP staining was positive as indicated by the arrows in mouse model while negative in controls 7 weeks later (× 100). **E** Bone damage by microCT were observed in the mouse model from lateral, coronal and sagittal scan at 7 weeks after the myeloma cell injection, compared with the controls. **F** Bar plots present the number of bone lytic lesions on the right medial tibia surface and the trabecular bone parameters: BMD, BV/TV, BS/BV, BS/TV, Tb.Th, Tb.Sp, Tb.N. Results are shown as mean ± SD. *P < 0.05, **P < 0.01, ***P < 0.001

was negatively correlated with these genes. Therefore, it is reasonable to hypothesize that C3a promotes MBD pathogenesis by inhibiting the expression of Sirt1 in osteoclasts, which in turn promotes osteoclast proliferation and function. This prompted us to conduct further experiments.

We then analyzed the numbers and fusion areas of osteoclasts after the addition of C3a in patients with NDMM, using TRAP staining. This once again confirmed the ability of C3a to stimulate the proliferation and differentiation of osteoclasts, along with a decrease in the level

of Sirt1 expression, as was seen earlier in our PCR and WB results. To verify the generalizability of these conclusions, we obtained consistent findings in the RAW264.7 cells. Cellular extracts from the RAW264.7 cells were collected for Co-IP experiments, and we observed that C3a and Sirt1 interacted. C3aR belongs to a family of G-protein-coupled receptors that are widely expressed in both organs and immune cells. C3aR and C5aR are expressed in human mesenchymal stem cells, osteoblasts, and osteoclasts. Therefore, it is reasonable to hypothesize that C3a promotes osteoclast proliferation by binding

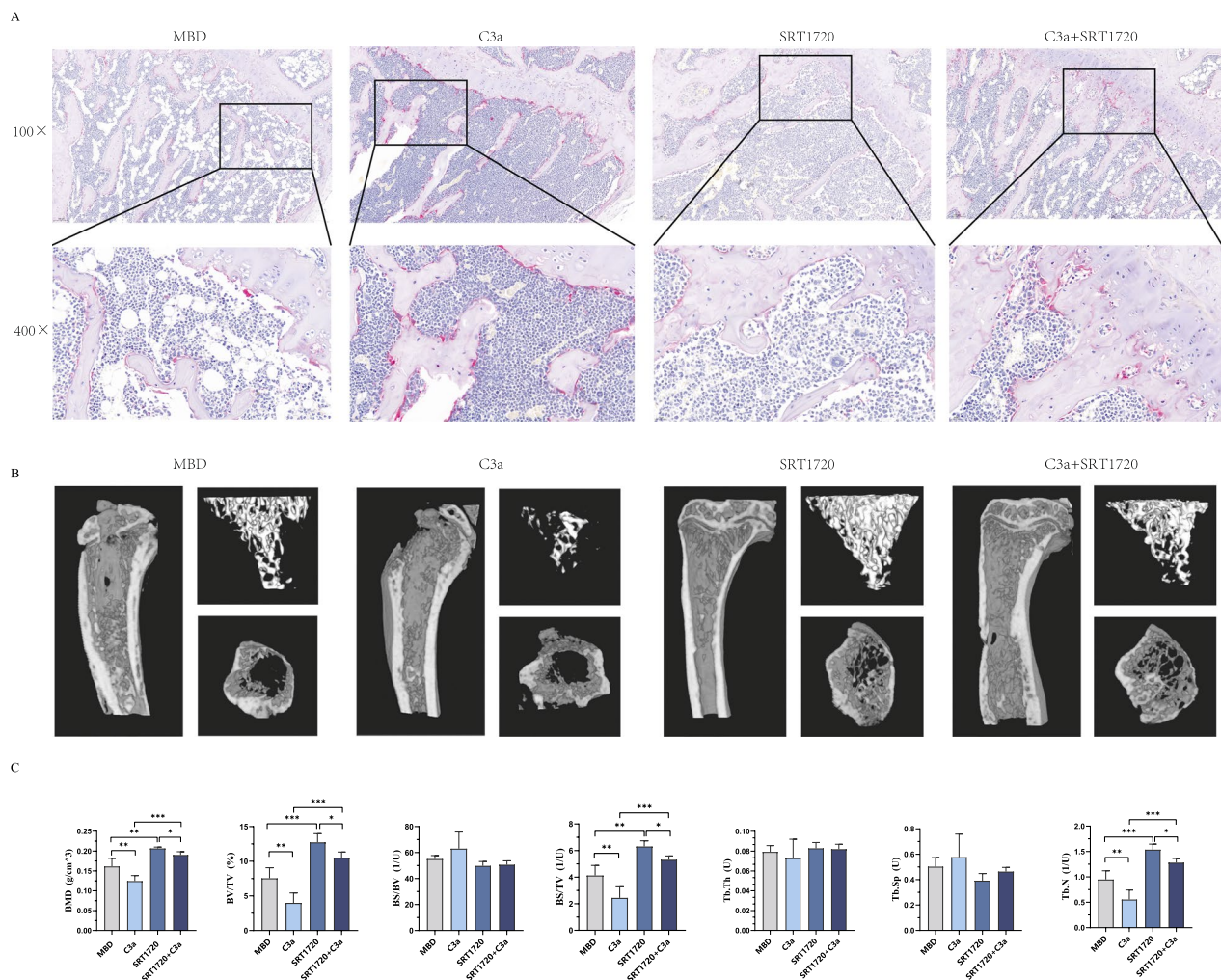


Fig. 7 In the MBD mouse model, complement C3a aggravated the bone disease in mice, and Sirt1 activator SRT1720 effectively attenuated the bone disease in mice. **A** Tibia sections were red after positive TRAP staining. (100×&400×) **B** Bone damage by microCT were observed in the mouse model from lateral, coronal and sagittal scan. **C** Bar plots present the number of bone lytic lesions on the right medial tibia surface and the trabecular bone parameters: BMD,BV/TV, BS/BV,BS/TV, Tb.Th, Tb.Sp, Tb.N. Results are shown as mean ± SD. *P < 0.05, **P < 0.01, ***P < 0.001

to the receptor, and thus to Sirt1 [38–40]. Several studies have shown that C3a interacts with Sirt1. Zhong et al. [41] demonstrated that the C3 activation products C3a and Asp play key roles in the development of hepatic steatosis, by regulating the expression of Gly-tRF via CYP2E1. Gly-tRFs promote lipogenesis and inhibit fatty-acid β-oxidation by regulating the Sirt1 signaling pathway in alcoholic fatty liver disease (AFLD), which reveals an interaction between C3a and Sirt1.

SRT 1720 is a selective activator of Sirt1, which shows less potent effects on Sirt2 and Sirt3 [42]. The addition of a Sirt1 activator in our study led to a decrease

in osteoclasts and downregulation of osteolysis-related markers, confirming our hypothesis. We wanted to continue exploring whether the Sirt1 activator could reverse the activating effect of C3a on osteoclasts, but the osteoclast fusion area and the expression of osteolysis-associated genes appeared to revert to the level of the unaddressed activator (i.e., the control) after the osteoclasts were cultured with the C3a and Sirt1 activator. However, it cannot be denied that activation of the Sirt1 gene in osteoclasts derived from patients with NDMM does inhibit osteoclasts and the osteolysis they induce. This is consistent with the results of previous studies on

Sirt1 [43]. A few findings have suggested that SRT1720 hinders bone resorption by disrupting the actin band of mature osteoclasts, inhibiting actin band formation and thus suppressing osteoclastogenesis—even in the absence of Sirt1 [44]. This implies that the mechanism of action of this compound goes beyond Sirt1 activation, potentially paving the way for new therapies for alleviating osteoporosis-related bone loss. However, it was only when the serum C3a levels of the patients were relatively high that the benefit of activating Sirt1 became less pronounced. This provides potential directions for future follow-up studies, wherein the use of Sirt1 activators in certain patients with myeloma and normal serum C3a levels may provide significant benefits.

In contrast, treatment with EX527 (a Sirt1 inhibitor) and Sirt1 silencing both promoted osteoclastogenesis [45]. In our study, the introduction of EX527 (a Sirt1 inhibitor) once again proved the antagonistic role of Sirt1 relative to osteoclast formation and showed that C3a and EX527 have a synergistic effect in activating osteoclasts. The same experiment was repeated in the cell lines, which was sufficient to prove the accuracy and reliability of our findings.

To further elucidate the relevant pathways involved, we performed RNA-seq analysis on RAW264.7 cells that overexpressed Sirt1 and compared them to control cells. Our previous studies demonstrated that C3a can activate osteoclasts through the PI3K/PDK1/SGK3 pathway; therefore, we focused on the PI3K-AKT and osteoclast differentiation pathways. By adding activators or inhibitors and overexpressing or knocking down Sirt1 in osteoclasts, we confirmed that complement C3a promoted osteoclast formation by inhibiting Sirt1 to activate the PI3K/PDK1/SGK3 pathway in patients with NDMM. Of course, other pathways regulate osteoclasts through Sirt1 as well. Studies have reported that the AMPK/SIRT1/NF- κ B pathway is associated with the formation of pro-inflammatory macrophages, as it affects the formation of neighboring osteoclasts by influencing their release of TNF- α [43, 46]. The conventional role of the targeted Sirt family was investigated. Sirt1 was observed to inhibit the deacetylation of p66Shc in osteoblasts and inhibit RANKL-induced osteoclastogenesis in the presence of stimulation with high glucose levels. Additionally, Sirt1 downregulation promotes osteoclast proliferation and bone resorption by regulating c-Fos and NFATc1 and enhancing endoplasmic reticulum stress [47].

In terms of in vivo experiments, our research team aimed to validate the therapeutic effect of Sirt1 activators on bone disease in an animal model of myeloma.

The injection of RPMI-8226 cells into the left tibia bone marrow cavities of NOD/SCID mice to construct a mouse model of MBD resulted in stable osteopathy at the injection site [48]. Micro-CT and pathological analysis results confirmed that Sirt1 activators exert a therapeutic effect on bone disease; however, the only two currently approved drugs for treating MBD are bisphosphonates and denosumab—a monoclonal antibody that inhibits RANKL [49]. Over the past several decades, proteasome inhibition has become an important therapeutic strategy for the treatment of MM and has improved the survival of patients with the condition [50]. Proteasome inhibition regulates bone metabolism by inhibiting RANKL-mediated osteoclast differentiation [51]. Bortezomib is a potent proteasome inhibitor that activates β -collagen/TCF signaling to induce osteoblast differentiation, upregulates RUNX-2 expression, and enhances osteoclastogenesis. Second-generation PIs such as ixazomib (MLN9708) represent the first oral PIs with robust levels of efficacy and a favorable safety profile, showing clinical benefits against myeloma bone disease by inhibiting bone resorption and promoting osteoclastogenesis [52, 53]. Estrogen can reduce the activation of OCs in the MM tumor microenvironment by affecting the PI3K-Akt pathway, leading to a reduction in the expression of the OC-regulating cytokines CCL2/3/4 [54]. Dairaghi et al. demonstrated the efficacy of a potent and orally bioavailable inhibitor of CCR1, one of the receptors for the chemokine CCL3/MIP-1, in murine models of MM and MBD [55, 56]. MLN3897, a specific antagonist of the chemokine receptor CCR1, impairs osteoclastogenesis and interferes with osteoclast-MM cell interactions in preclinical settings [57].

The root cause of myeloma bone disease lies in the myeloma cells, and as shown previously, some drugs used to treat myeloma have been shown to have a modulating effect on osteoclasts and osteoblasts thereby ameliorating bone damage. A number of small molecule drugs are also being developed, all of which offer new hope for the improvement of myeloma bone disease. Preclinical trials of novel drugs in populations are continuing, and there is a need to continue to explore new mechanisms for traditional drugs and whether combinations of drugs can provide benefit to patients with myeloma bone disease. We will further investigate the role of Sirt1 activators in the treatment of MBD. Overall (Fig. 8), we observed that complement C3a activated osteoclasts by inhibiting Sirt1 to activate the PI3K/PDK1/SGK3 pathway in patients with MM, which was reduced by treatment with a Sirt1

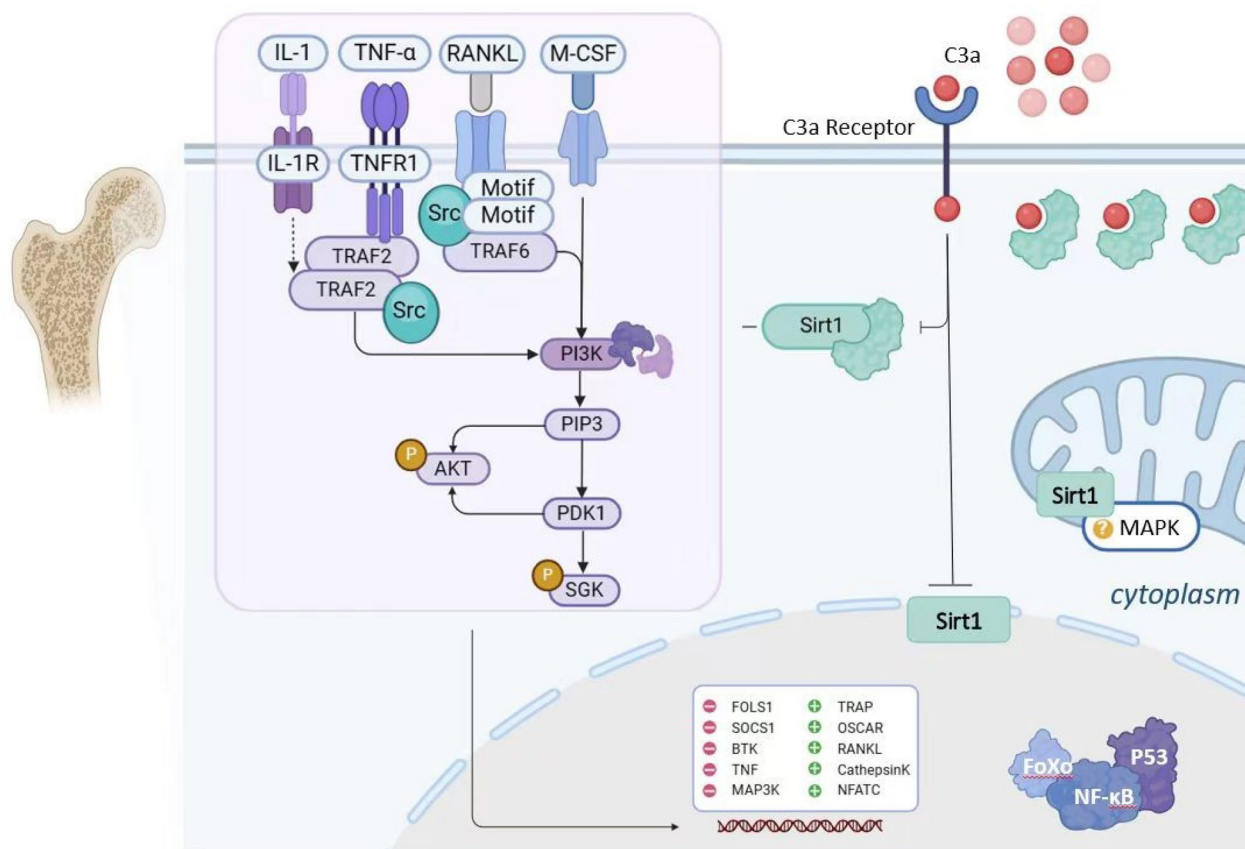


Fig. 8 Complement C3a promotes the formation of osteoclasts by inhibiting Sirt1 to activate the PI3K/PDK1/SGK3 pathway in patients with multiple myeloma

activator. This study identified new potential therapeutic targets and strategies for treating patients with MBD.

Conclusions

Complement C3a inhibits Sirt1 activation of the PI3K/PDK1/SGK3 pathway, which promotes osteoclast formation in MM patients. The use of Sirt1 activators may reduce osteoclast formation and decrease the severity of bone disease, which is promising for the treatment of MBD. In conclusion, this study provides new potential therapeutic targets and strategies for patients with myeloma bone disease.

Abbreviations

NDMM	Newly diagnosed multiple myeloma
HD	Healthy donors
MBD	Myeloma bone disease
MM	Multiple myeloma
Sirts	Sirtuins
BMMCs	Bone marrow mononuclear cells
OCs	Osteoclasts
OCPs	Osteoclast precursors
C3a	Complement C3a

C3aR	Complement C3a
CTX	C-terminal cross-linking telopeptide of type I collagen
TRACP-5b	Tartrate-resistant acid phosphatase 5b
TRAP	Tartrate-resistant acid phosphatase
OSCAR	Osteoclast-associated receptor
RANKL	Receptor activator of nuclear factor-kappa B ligand
CTSK	Cathepsin K
Co-IP	Co-immunoprecipitation
R-ISS	Revised international staging system
FPKM	Fragments Per Kilobase of exon model per Million mapped fragments

Supplementary Information

The online version contains supplementary material available at <https://doi.org/10.1186/s12967-025-06319-3>.

- Supplementary material 1.
- Supplementary material 2.

Acknowledgements

We thank all the participants who took part in this study.

Author contributions

RF, ZL, FJ designed the experiments and revised the manuscript. FJ and YZ performed experiments and analyzed the data. FP, HL, KD, PC, XLand LL contributed to reagents/materials/analysis tools and collection of patients’

features. FJ and YZ wrote the paper. All authors contributed to the final version of the manuscript and approved it for publication.

Funding

This work was sponsored by Tianjin Health Research Project (Grant No. TJWJ2024QN008), the Tianjin Municipal Natural Science Foundation (Grant No. 23JCQNJC00870), the National Natural Science Foundation of China (Grant No. 82000219).

Availability of data and materials

The datasets used and/or analyzed during the current study are available from the corresponding author on reasonable request. All materials used in the study are listed in the Methods section and are available to other researchers for replication of the study.

Declarations

Ethics approval and consent to participate

This study was conducted in accordance with the ethical standards as laid down in the 1964 Declaration of Helsinki and its later amendments. Ethical approval was obtained from the the Ethics Committee of Tianjin Medical University with the approval number IRB2020-KY-109.

Consent for publication

Informed consent for publication was obtained from all participants, or their legal guardians, in cases where the study involved minors or patients unable to provide consent. Any potentially identifying images have been removed or anonymized.

Competing interests

The authors declare that they have no competing interests.

Author details

¹Department of Hematology, Tianjin Medical University General Hospital, 154 Anshan Street, Heping District, Tianjin 300052, China. ²Tianjin Key Laboratory of Bone Marrow Failure and Malignant Hemopoietic Clone Control, Tianjin 300052, China. ³Tianjin Institute of Hematology, Tianjin 300052, China.

Received: 16 January 2025 Accepted: 24 February 2025

Published online: 16 March 2025

References

- Terpos E, Ntanasis-Stathopoulos I, Dimopoulos MA. Myeloma bone disease: from biology findings to treatment approaches. *Blood*. 2019;133:1534–9.
- Callander NS, Baljevic M, Adekola K, Anderson LD, Campagnaro E, Castillo JJ, Costello C, Devarakonda S, Elsedawy N, Fairman M, et al. NCCN Guidelines[®] Insights: Multiple Myeloma, Version 3.2022. *J Natl Compr Canc Netw*. 2022;20:8–19.
- Rajkumar SV. Multiple myeloma: 2022 update on diagnosis, risk stratification, and management. *Am J Hematol*. 2022;97:1086–107.
- Diaz-delCastillo M, Chantry AD, Lawson MA, Heegaard AM. Multiple myeloma-A painful disease of the bone marrow. *Semin Cell Dev Biol*. 2021;112:49–58.
- Lungu O, Toscani D, Burroughs-Garcia J, Giuliani N. The metabolic features of osteoblasts: implications for multiple myeloma (MM) bone disease. *Int J Mol Sci*. 2023;24:4893.
- Fu R, Liu H, Zhao S, Wang Y, Li L, Gao S, Ruan E, Wang G, Wang H, Song J, Shao Z. Osteoblast inhibition by chemokine cytokine ligand3 in myeloma-induced bone disease. *Cancer Cell Int*. 2014;14:132.
- Jiang F, Liu H, Liu Z, Song J, Li L, Ding K, Ren Y, Peng F, Shao Z, Fu R. High serum levels of complements C3 and C4 as novel markers for myeloma bone disease. *Ann Hematol*. 2017;96:331–3.
- Jiang F, Liu H, Peng F, Liu Z, Ding K, Song J, Li L, Chen J, Shao Q, Yan S, et al. Complement C3a activates osteoclasts by regulating the PI3K/PDK1/SGK3 pathway in patients with multiple myeloma. *Cancer Biol Med*. 2021;18:721–33.
- Cantley MD, Zannettino ACW, Bartold PM, Fairlie DP, Haynes DR. Histone deacetylases (HDAC) in physiological and pathological bone remodelling. *Bone*. 2017;95:162–74.
- Yi T, Baek JH, Kim HJ, Choi MH, Seo SB, Ryoo HM, Kim GS, Woo KM. Trichostatin A-mediated upregulation of p21(WAF1) contributes to osteoclast apoptosis. *Exp Mol Med*. 2007;39:213–21.
- Bradley EW, Carpio LR, van Wijnen AJ, McGee-Lawrence ME, Westendorf JJ. Histone deacetylases in bone development and skeletal disorders. *Physiol Rev*. 2015;95:1359–81.
- Edwards JR, Perrien DS, Fleming N, Nyman JS, Ono K, Connelly L, Moore MM, Lwin ST, Yull FE, Mundy GR, Eleftheriou F. Silent information regulator (Sir)T1 inhibits NF- κ B signaling to maintain normal skeletal remodeling. *J Bone Miner Res*. 2013;28:960–9.
- Shakibaei M, Buhmann C, Mobasheri A. Resveratrol-mediated SIRT-1 interactions with p300 modulate receptor activator of NF- κ B ligand (RANKL) activation of NF- κ B signaling and inhibit osteoclastogenesis in bone-derived cells. *J Biol Chem*. 2011;286:11492–505.
- Venkateshaiah SU, Khan S, Ling W, Bam R, Li X, van Rhee F, Usmani S, Barlogie B, Epstein J, Yaccoby S. NAMPT/PBEF1 enzymatic activity is indispensable for myeloma cell growth and osteoclast activity. *Exp Hematol*. 2013;41:547–557.e542.
- Yamamoto T, Tamaki K, Shirakawa K, Ito K, Yan X, Katsumata Y, Anzai A, Matsuhashi T, Endo J, Inaba T, et al. Cardiac Sirt1 mediates the cardio-protective effect of caloric restriction by suppressing local complement system activation after ischemia-reperfusion. *Am J Physiol Heart Circ Physiol*. 2016;310:H1003–1014.
- Gillum MP, Kotas ME, Erion DM, Kursawe R, Chatterjee P, Nead KT, Muise ES, Hsiao JJ, Frederick DW, Yonemitsu S, et al. SirT1 regulates adipose tissue inflammation. *Diabetes*. 2011;60:3235–45.
- Bolasco G, Calogero R, Carrara M, Banachabouchi MA, Bilbao D, Mazzoccoli G, Vinciguerra M. Cardioprotective mIGF-1/SIRT1 signaling induces hypertension, leukocytosis and fear response in mice. *Aging (Albany NY)*. 2012;4:402–16.
- Ehrnthaller C, Huber-Lang M, Nilsson P, Bindl R, Redeker S, Recknagel S, Rapp A, Mollnes T, Amling M, Gebhard F, Ignatius A. Complement C3 and C5 deficiency affects fracture healing. *PLoS One*. 2013;8:e81341.
- Tu Z, Bu H, Dennis JE, Lin F. Efficient osteoclast differentiation requires local complement activation. *Blood*. 2010;116:4456–63.
- Sato T, Abe E, Jin CH, Hong MH, Katagiri T, Kinoshita T, Amizuka N, Ozawa H, Suda T. The biological roles of the third component of complement in osteoclast formation. *Endocrinology*. 1993;133:397–404.
- Ignatius A, Schoengraf P, Kreja L, Liedert A, Recknagel S, Kandert S, Brenner RE, Schneider M, Lambris JD, Huber-Lang M. Complement C3a and C5a modulate osteoclast formation and inflammatory response of osteoblasts in synergism with IL-1 β . *J Cell Biochem*. 2011;112:2594–605.
- Kovtun A, Bergdolt S, Hägele Y, Matthes R, Lambris JD, Huber-Lang M, Ignatius A. Complement receptors C5aR1 and C5aR2 act differentially during the early immune response after bone fracture but are similarly involved in bone repair. *Sci Rep*. 2017;7:14061.
- Rajkumar SV, Dimopoulos MA, Palumbo A, Blade J, Merlini G, Mateos MV, Kumar S, Hillengass J, Kastritis E, Richardson P, et al. International Myeloma Working Group updated criteria for the diagnosis of multiple myeloma. *Lancet Oncol*. 2014;15:e538–548.
- Palumbo A, Avet-Loiseau H, Oliva S, Lokhorst HM, Goldschmidt H, Rosinol L, Richardson P, Caltagirone S, Lahuerta JJ, Facon T, et al. Revised International Staging System for Multiple Myeloma: A Report From International Myeloma Working Group. *J Clin Oncol*. 2015;33:2863–9.
- Song C, Yang X, Lei Y, Zhang Z, Smith W, Yan J, Kong L. Evaluation of efficacy on RANKL induced osteoclast from RAW264.7 cells. *J Cell Physiol*. 2019;234:11969–75.
- Fu R, Peng F, Liu H, Wang Y, Li L, Wang G, Song J, Shao Z. Clinical significance of osteoblast precursors and osteoclast precursors in earlier diagnosis and monitoring of myeloma bone disease. *Ann Hematol*. 2016;95:1099–106.
- Boyce BF. Advances in the regulation of osteoclasts and osteoclast functions. *J Dent Res*. 2013;92:860–7.
- Mellis DJ, Itzstein C, Helfrich MH, Crockett JC. The skeleton: a multi-functional complex organ: the role of key signalling pathways in osteoclast differentiation and in bone resorption. *J Endocrinol*. 2011;211:131–43.
- Liu H, Peng F, Liu Z, Jiang F, Li L, Gao S, Wang G, Song J, Ruan E, Shao Z, Fu R. CYR61/CCN1 stimulates proliferation and differentiation of osteoblasts

- in vitro and contributes to bone remodeling in vivo in myeloma bone disease. *Int J Oncol*. 2017;50:631–9.
30. Gai D, Chen JR, Stewart JP, Nookaew I, Habelhah H, Ashby C, Sun F, Cheng Y, Li C, Xu H, et al. CST6 suppresses osteolytic bone disease in multiple myeloma by blocking osteoclast differentiation. *J Clin Invest*. 2022. <https://doi.org/10.1172/JCI159527>.
 31. Wang D, Wang J, Zheng X, Diao S, Li W, Ma W. Bone homeostasis disorders increased the mortality of sepsis patients: a preliminary retrospective cohort study. *Front Med (Lausanne)*. 2022;9:1017411.
 32. Chubb SA. Measurement of C-terminal telopeptide of type I collagen (CTX) in serum. *Clin Biochem*. 2012;45:928–35.
 33. Terpos E, de la Fuente J, Szydlo R, Hatjiharissi E, Viniou N, Meletis J, Yata-ganas X, Goldman JM, Rahemtulla A. Tartrate-resistant acid phosphatase isoform 5b: a novel serum marker for monitoring bone disease in multiple myeloma. *Int J Cancer*. 2003;106:455–7.
 34. Woitge HW, Horn E, Keck AV, Auler B, Seibel MJ, Pecherstorfer M. Biochemical markers of bone formation in patients with plasma cell dyscrasias and benign osteoporosis. *Clin Chem*. 2001;47:686–93.
 35. Lund T, Abildgaard N, Andersen TL, Delaisse JM, Plesner T. Multiple myeloma: changes in serum C-terminal telopeptide of collagen type I and bone-specific alkaline phosphatase can be used in daily practice to detect imminent osteolysis. *Eur J Haematol*. 2010;84:412–20.
 36. Kowalska M, Druzd-Sitek A, Fuksiewicz M, Kotowicz B, Chechlinska M, Szczywska M, Walewski J, Kaminska J. Procollagen I amino-terminal propeptide as a potential marker for multiple myeloma. *Clin Biochem*. 2010;43:604–8.
 37. D'Amelio P, Tamone C, Sassi F, D'Amico L, Roato I, Patanè S, Ravazzoli M, Veneziano L, Ferracini R, Pescarmona GP, Isaia GC. Teriparatide increases the maturation of circulating osteoblast precursors. *Osteoporos Int*. 2012;23:1245–53.
 38. Zhang L, Bao D, Li P, Lu Z, Pang L, Chen Z, Guo H, Gao Z, Jin Q. Particle-induced SIRT1 downregulation promotes osteoclastogenesis and osteolysis through ER stress regulation. *Biomed Pharmacother*. 2018;104:300–6.
 39. McCarty MF, Lewis Lujan L, Assanga SI. Targeting Sirt1, AMPK, Nrf2, CK2, and soluble guanylate cyclase with nutraceuticals: a practical strategy for preserving bone mass. *Int J Mol Sci*. 2022;23:4776.
 40. Kim HN, Iyer S, Ring R, Almeida M. The role of FoxOs in bone health and disease. *Curr Top Dev Biol*. 2018;127:149–63.
 41. Zhong F, Hu Z, Jiang K, Lei B, Wu Z, Yuan G, Luo H, Dong C, Tang B, Zheng C, et al. Complement C3 activation regulates the production of tRNA-derived fragments Gly-tRFs and promotes alcohol-induced liver injury and steatosis. *Cell Res*. 2019;29:548–61.
 42. Milne JC, Lambert PD, Schenk S, Carney DP, Smith JJ, Gagne DJ, Jin L, Boss O, Perni RB, Vu CB, et al. Small molecule activators of SIRT1 as therapeutics for the treatment of type 2 diabetes. *Nature*. 2007;450:712–6.
 43. Ye Q, Xu H, Liu S, Li Z, Zhou J, Ding F, Zhang X, Wang Y, Jin Y, Wang Q. Apoptotic extracellular vesicles alleviate Pg-LPS induced inflammatory responses of macrophages via AMPK/SIRT1/NF- κ B pathway and inhibit osteoclast formation. *J Periodontol*. 2022;93:1738–51.
 44. Thiyagarajan R, Gonzalez MR, Zaw C, Seldeen KL, Hernandez M, Pang M, Troen BR. SRT2183 and SRT1720, but not resveratrol, inhibit osteoclast formation and resorption in the presence or absence of Sirt1. *J Bone Res*. 2023;11:1000235.
 45. Tao Z, Tao M, Zhou M, Wu XJ. Niacin treatment prevents bone loss in iron overload osteoporotic rats via activation of SIRT1 signaling pathway. *Chem Biol Interact*. 2024;388:110827.
 46. Yan S, Miao L, Lu Y, Wang L. Sirtuin 1 inhibits TNF- α -mediated osteoclastogenesis of bone marrow-derived macrophages through both ROS generation and TRPV1 activation. *Mol Cell Biochem*. 2019;455:135–45.
 47. Qu B, Gong K, Yang H, Li Y, Jiang T, Zeng Z, Cao Z, Pan X. SIRT1 suppresses high glucose and palmitate-induced osteoclast differentiation via deacetylating p66Shc. *Mol Cell Endocrinol*. 2018;474:97–104.
 48. Mehdi SH, Morris CA, Lee JA, Yoon D. An improved animal model of multiple myeloma bone disease. *Cancers*. 2021;13:4277.
 49. Roodman GD. Pathogenesis of myeloma bone disease. *Blood Cells Mol Dis*. 2004;32:290–2.
 50. Terpos E, Zamagni E, Lentzsch S, Drake MT, Garcia-Sanz R, Abildgaard N, Ntanasis-Stathopoulos I, Schjesvold F, de la Rubia J, Kyriakou C, et al. Treatment of multiple myeloma-related bone disease: recommendations from the Bone Working Group of the International Myeloma Working Group. *Lancet Oncol*. 2021;22:e119–30.
 51. Terpos E, Sezer O, Croucher P, Dimopoulos MA. Myeloma bone disease and proteasome inhibition therapies. *Blood*. 2007;110:1098–104.
 52. Pennisi A, Li X, Ling W, Khan S, Zangari M, Yaccoby S. The proteasome inhibitor, bortezomib suppresses primary myeloma and stimulates bone formation in myelomatous and nonmyelomatous bones in vivo. *Am J Hematol*. 2009;84:6–14.
 53. Qiang YW, Heuck CJ, Shaughnessy JD Jr, Barlogie B, Epstein J. Proteasome inhibitors and bone disease. *Semin Hematol*. 2012;49:243–8.
 54. Cui Y, Wang F, Zhang D, Huang J, Yang Y, Xu J, Gao Y, Ding H, Qu Y, Zhang W, et al. Estrogen-responsive gene MAST4 regulates myeloma bone disease. *J Bone Miner Res*. 2022;37:711–23.
 55. Dairaghi DJ, Oyajobi BO, Gupta A, McCluskey B, Miao S, Powers JP, Seitz LC, Wang Y, Zeng Y, Zhang P, et al. CCR1 blockade reduces tumor burden and osteolysis in vivo in a mouse model of myeloma bone disease. *Blood*. 2012;120:1449–57.
 56. Sebag M. CCR1 blockade and myeloma bone disease. *Blood*. 2012;120:1351–2.
 57. Vallet S, Raje N, Ishitsuka K, Hideshima T, Podar K, Chhetri S, Pozzi S, Breitkreutz I, Kiziltepe T, Yasui H, et al. MLN3897, a novel CCR1 inhibitor, impairs osteoclastogenesis and inhibits the interaction of multiple myeloma cells and osteoclasts. *Blood*. 2007;110:3744–52.

Publisher's Note

Springer Nature remains neutral with regard to jurisdictional claims in published maps and institutional affiliations.